

THE UNIVERSITY OF CALGARY

Stereomammography

by

Hilary Alto

A THESIS

SUBMITTED TO THE FACULTY OF GRADUATE STUDIES  
IN PARTIAL FULFILMENT OF THE REQUIREMENTS FOR THE  
DEGREE OF MASTER OF SCIENCE

DEPARTMENT OF GEOMATICS ENGINEERING

CALGARY, ALBERTA

DECEMBER, 1995

© Hilary Alto 1995

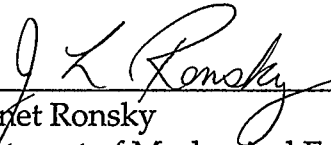
THE UNIVERSITY OF CALGARY  
FACULTY OF GRADUATE STUDIES

The undersigned certify that they have read, and recommend to the Faculty of Graduate Studies for acceptance, a thesis entitled "Stereomammography" submitted by Hilary Alto in partial fulfilment of the requirements for the degree of Master of Science.



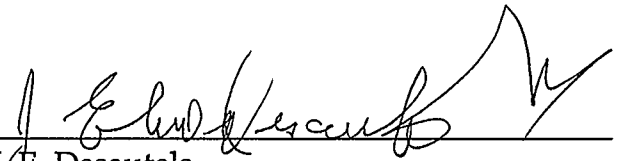
---

Supervisor, Dr. M. A. Chapman  
Department of Geomatics Engineering



---

Dr. Janet Ronsky  
Department of Mechanical Engineering



---

Dr. J. E. Desautels  
Associate, Drs. May, Yemen and Associates

December 14, 1995  
Date

## ABSTRACT

Breast cancer will affect one in ten Canadian women during their lifetime. Mammography is used to detect breast cancer in its earliest stages. Clusters of microcalcifications are primary indicators of breast cancer. The shape, size and number of these calcifications may be used to determine whether they are malignant or benign. However, overlapping images of calcifications on a mammogram hinder the classification of the shape and size of each calcification and a misdiagnosis may result. Three-dimensional mathematical object reconstruction can be utilised to separate the calcifications, thereby allowing for a more accurate classification.

A Plexiglas phantom, embedded with 1 mm lead pellets, was surveyed and filmed mammographically. The photogrammetric techniques of relative and absolute orientation were applied to the two dimensional mammograms. A three-dimensional depth map was analytically generated with an overall accuracy of 0.6 mm. A Bundle Adjustment and Direct Linear Transformation confirmed the results.

## ACKNOWLEDGEMENTS

I would like to take this opportunity to recognise and thank all the people who helped and supported me throughout my Master's studies.

First of all, I wish to thank Dr. Chapman for his encouragement in my entering the Department of Geomatics Engineering as well as for his supervision and support.

Others who were instrumental in the success of the research include:

Dr. Desautels for suggesting this thesis topic and for arranging for my work at Screen Test Alberta as well as getting clinical mammograms from Dr. Horezcko in Edmonton.

Caroline Resner, without whom this research would never have happened. For her enthusiasm in the construction of the phantom and her willingness to spend many long Sunday afternoons imaging it.

Delbert Caveny, the creator of the phantom and the film table that were so necessary to this thesis.

Dr. Bryant for her interest and support in this research and her permission to conduct the imaging at Screen Test Alberta.

Vladimir Argesenau, Radoslav Gaidajev and Derek Lichti who did such a great job of surveying the cube/phantom.

Hamid Ebadi and Christian Larouche for all of their help with the Bundle and DLT programs.

Dr. Blais who throughout my studies was always there to answer questions on anything and everything that I did not understand.

The secretaries in the Department of Geomatics Engineering, especially Anne Gehring for her assistance with all the paperwork and deadlines.

Terry Labach for his assistance with my programming questions and data storage problems.

Shirley Matile, who so carefully read the first draft of this thesis.

*Dedicated to*  
*Jussi, Jaime, Owen and Kevin*  
*for their love, patience and support*

## TABLE OF CONTENTS

APPROVAL PAGE .....	ii
ABSTRACT .....	iii
ACKNOWLEDGEMENTS .....	iv
DEDICATION .....	vi
TABLE OF CONTENTS.....	vii
LIST OF TABLES.....	x
LIST OF FIGURES.....	xi

### Chapter

1 Introduction .....	1
1.1 Motivation .....	2
2 Mammography.....	9
2.1 Physics of Mammography .....	12
2.2 Physics of X-Ray Generation.....	16
2.2.1 Components of an X-Ray Tube .....	18
2.2.2 Geometry of X-Ray Source .....	21
2.3 Mammographic Equipment.....	23
2.4 Breast Cancer Features Visible on Mammograms .....	25

2.5	Requirements for Quality Images .....	29
3	X-Ray Photogrammetry .....	32
3.1	Principles of X-Ray Photogrammetry .....	33
3.2	Application of X-Ray Photogrammetry to Mammography .....	38
3.3	Benefits of Stereo Viewing in Mammography .....	39
4	Phantom Construction and Calibration .....	41
4.1.	Choice of Materials for a Phantom.....	42
4.2	Choice of Shape and Size of the Phantom .....	43
4.3	Microsurvey of Phantom.....	45
4.4	Error Analysis .....	47
4.5	Estimated Phantom Coordinates.....	52
5	Stereomammographic Imaging of Phantom.....	54
5.1	Stereo-Imaging Methodology .....	54
5.2	Film and Other Considerations .....	55
5.3	Orientation of the Phantom .....	56
5.4	Coordinate Determination of Pellets on Images .....	57
5.5	Resolution of the Images .....	58
6	Object Reconstruction .....	59
6.1	Application of Photogrammetry to Object Reconstruction.....	59
6.2	Mathematical Model of Photogrammetric Configuration.....	63



6.3 Mathematical Reconstruction of the Model.....	77
7 Conclusions and Recommendations.....	88
7.1 Conclusions .....	88
7.2 Recommendations.....	90
References .....	93

## LIST OF TABLES

### TABLE

1.1 Tumour Diameter versus Metastasis Probability .....	3
4.1 Final Control Point Coordinates .....	53
6.1 Calculated Centre Coordinates and Radii.....	68
6.2 Average Values of Fiducials.....	69
6.3 Principal Points Calculated from DLT (first run).....	70
6.4 Principal Points Calculated from DLT (last run).....	71
6.5 Image Coordinates Corrected for Centre of Gravity and Principal Point Shift.....	79
6.6 DLT Results Using All Three Films .....	80
6.7 Model Coordinates Using Left and Right Film .....	81
6.8 Model Coordinates Using Left and Middle Film .....	82
6.9 Model Coordinates Using Middle and Right Film.....	83
6.10 Final Results of Absolute Orientation.....	84
6.11 Exterior Orientation Parameters from Bundle Adjustment.....	85
6.12 Interior Orientation Parameters .....	85
6.13 Mathematical Model Fit.....	86
6.14 Accuracy of the Models .....	86

## LIST OF FIGURES

### FIGURE

2.1	Detail of Anode and Cathode Configuration.....	10
2.2	Components of a Typical Mammography Device.....	11
2.3	Typical Wavelength and Frequency Ranges.....	12
2.4	Attenuation Coefficient versus X-ray Photon Energy .....	15
2.5	Anode Angle.....	20
2.6	Diagram of Heel Effect.....	22
2.7	Assembly of Source/ Anode and Film Plane .....	24
2.8	LORAD M-III System.....	25
2.9	Cranio Caudad and Medio-Lateral Views .....	27
3.1	Diagram of Interior Orientation.....	36
4.1	Diagram of Plexiglas Phantom.....	43
4.2	Theodolite Stations and Phantom Position .....	47
5.1	Film Acquisition Configuration .....	55
5.2	Phantom on Film Table.....	56
6.1	Diagrams of Phantom Features on Films .....	60
6.2	Centre of Ellipse versus Centre of Circle.....	62
6.3	Diagram of Image Acquisition Configuration.....	64
6.4	Relative Placement of Films in the Wild AC1 Stereo Comparator .....	72

6.5	Vector of $A \times B$ .....	73
6.6	Diagram of Geometry of $(A \times B) \bullet C$ .....	73

## CHAPTER ONE

### INTRODUCTION

Neither the principles of photogrammetry and image processing nor mathematical object reconstruction have been applied to mammography in the past. With the continued concern over the incidence of breast cancer and no immediate cure in sight, any and all methods should be applied in order to detect breast cancer in its earliest form.

The purpose of this thesis is to research the application of photogrammetric techniques/principles of stereo-viewing and three-dimensional object reconstruction to mammographic images of pseudo (man-made) calcifications. A three-dimensional depth map will be created for the object which is a phantom (representing a female breast) of known dimensions. This depth map will be used to give depth-perception to an otherwise two-dimensional, or monocular, image. It is hoped that this work will enhance the work of Liang Shen (1992) in the Electrical Department on classification of calcifications.

The basic concepts and techniques of mammography and its use in the screening and diagnosis of breast cancer will be covered. X-ray photogrammetry and its application to mammography will also be described.

The engineering aspects of photogrammetry, including the calibration of the phantom and the imaging techniques used to acquire meaningful data for the

final reconstruction process, will be reviewed. The mathematical methods and models chosen to represent the object and the processes used in this research will be described in detail .

The conclusions and recommendations will confirm that photogrammetry is a viable method for reconstructing a three-dimensional object which has been imaged with a mammography machine. Suggestions as to the changes in the machinery and the protocol of acquiring the mammograms will be made.

## 1.1 MOTIVATION

Breast cancer will affect one in ten Canadian women and one in nine American women during their lifetime. The number of women being diagnosed with breast cancer is increasing steadily with 4300 Canadian women dying from the disease each year. Breast cancer is devastating to those diagnosed with the disease. It is just as devastating to their loved ones because breast cancer is a relatively slow and painful disease. Often, the detection of cancer results in surgery. This can leave the woman disfigured for the rest of her life. There is no cure or known preventative measures and all people touched by this disease feel helpless. The only confirmed action is to detect the breast cancer at its earliest stages before it has metastasised (spread). Therefore, better imaging methods for screening and diagnosis are needed to improve the chances of early detection. Recently, in a paper by Sivaramakrishna [1995], the probability of

metastasis in cases of breast cancer with respect to tumour size was assessed. The results show that the relationship between metastasis and tumour size is log-normal. This means that the larger the tumour, the probability of metastasis increases very rapidly (see Table 1.1). It also indicates that the smaller the tumour, the probability drops just as rapidly. Therefore, the sooner the cancer is discovered, the better the prognosis for recovery will be.

**Table 1.1**  
**Tumour Diameter versus Metastasis Probability**  
from Sivaramakrishna [1995]

Diameter (cm)	Metastasis Probability (%)
1	7
0.5	1
0.4	0.56
0.3	0.20
0.2	0.04

There have been some improvements to the methods of breast cancer screening with respect to reduced exposure to radiation. Surprisingly, the actual techniques or protocols used in mammography have remained largely unchanged over the last thirty years. Stereotactic methods of imaging the breast (i.e., 3-D viewing) have been used successfully for many years for diagnosis and treatment planning.

The incidence of breast cancer has steadily increased since the 1940's. Fortunately, the mortality rate has remained stable. The use of mammography

has improved the detection capability to 0.7 per 1000 for small non-palpable cancers [Ciatto et al, 1987]. Early detection can lead to more successful treatment and longer survival rates after diagnosis. Results from screening programs for women over the age of fifty that have been followed for 10 to 18 years, indicate that there is actually a 25% reduction in mortality [Fletcher et al, 1993].

Mammography is the technique of imaging the breast using low-dose radiation and special x-ray films. Even with new technological advances and computer capabilities, the mammogram is still the most reliable method for the early detection of breast cancer [Shen, 1993]. The mammogram, with its low operating cost and high resolution images, for certain groups of women, has disadvantages. For example, women under the age of fifty have breasts that are too dense. This means that the films do not exhibit enough contrast to be effective in detecting cancerous growths or calcifications. Therefore, screening programs for the detection of breast cancer are directed at women over the age of fifty. Another disadvantage is that only two-dimensional images are created at approximately 90 degrees to each other thus making three-dimensional viewing or the capability of depth perception, impossible. These two-dimensional images have been the preferred configuration for radiologists for the last thirty years even though three-dimensional imaging as a tool has been available in other scientific applications for many years.



To address the issue of interpreting two-dimensional images, two groups of people, mostly in North America, are concentrating on 3-D imaging of the breast. One group is using Magnetic Resonance Imaging (MRI) and Computed Tomography (CT) images, while the other is using digital images created from the x-ray mammographic procedures and applying image processing techniques. MRI and CT, when used together, work well. MRI is used for imaging soft tissue and, therefore, improves the detection of lumps. CT, which is used to image density differences, improves the detection of calcifications (e.g., calcifications have much higher densities than soft tissue) [Zhou, 1989]. A true three-dimensional representation will result due to the slice images acquired by the MRI and CT machines. However, the procedures and apparatus are expensive and cumbersome and their resolution is not sufficiently fine at present to be used for the detection of very small micro-calcifications. The digital images and image processing techniques applied to mammography by one researcher in the United States are computationally demanding [Chelberg, 1994]. The high resolution images that are necessary for the detection of micro-calcifications result in very large image files and the produced depth map has questionable precision for the location of tumours or calcifications. Until the new methods are proven to be cost-effective, more accurate and easily adapted, they will not be accepted by the medical community at large.

Therefore, it is reasonable to continue to improve existing technologies and equipment until the newer methods are proven to be more effective. It was with this belief that the research presented here utilised the concepts of x-ray photogrammetry and the existing apparatus.

X-ray photogrammetry has been successfully applied to many medical problems from scoliosis to cosmetic reconstruction. Stereotactic methods, using photogrammetric principles have also been used for years in the treatment planning stage (e.g., biopsy) of breast cancer. By shifting the film between exposures so that the images do not overlap 100%, stereo images are created. A special attachment is required to apply stereotactic methods. The Foothills Hospital, Calgary has the required attachment but many of the mammographic machines in use today, do not. This is due to cost and availability of the attachment as well as the type of mammography that is being performed. As mentioned earlier, stereotactic imaging is used solely for diagnosis and treatment of suspected breast cancer and not for screening purposes. Therefore, the machine at Screen Test in Calgary which is used only for screening purposes, does not have the attachment. An adaptation to the machine was developed and is described in Chapter 5.

The most important contribution that photogrammetry can make to mammography is to create images that are more meaningful to the radiologist. Ultimately, this means creating a three-dimensional image rather than a two-

dimensional image. A stereo imaging method is currently used in Edmonton for needle biopsies. The disadvantages for the existing 3-dimensional methods (e.g., CT, MRI and stereotactic mammography) include a poor precision of approximately one centimetre and still no means for visually creating a depth map to enhance the ability of the radiologist to read the relative locations of the tumours/lesions. Studies in stereo vision have proven that the inclusion of depth information improves the recognition capabilities of interpreters for radiology as well as in topography related digital image processing [Chelberg, 1994].

Mammography is also the imaging method of choice for screening and for the detection and initial diagnosis of non-palpable breast cancer. As explained earlier, it is the most cost-effective and reliable method for the detection of breast cancer. "Mammography is the only examination capable of depicting malignant calcifications in the breast" [Bassett, 1992].

Research related to calcification classification using mammography is currently being undertaken by Liang Shen in the Electrical Engineering Department at the University of Calgary. He is classifying the sizes and shapes of micro-calcifications that are imaged (i.e., visible) in the mammograms, to identify potential malignancies in the breast. If the edges of the microcalcifications are rough and irregular, it has been found that they have a high incidence of being malignant. Conversely, if the calcifications are large and

smooth, they are usually benign. Therefore, the differentiation between the calcifications becomes important to the diagnosis [Shen, 1993].

With a two-dimensional image, some micro-calcifications can appear overlapped. This results in a false positive classification due to the shape and size of the visible calcification. Alternatively, a malignant calcification may be completely occluded from view by a larger calcification and a false negative diagnosis would be returned. This would result in the malignancy being left in place to metastasise unnoticed.

With the combination of the stereo viewing and the calcification classification being performed by researchers such as Liang Shen, the occurrence of false diagnoses will be reduced.

## CHAPTER TWO

### MAMMOGRAPHY

Mammography is the technique used in the imaging of the breast for the early detection of non-palpable breast cancer. To date, it is the most effective and economical method available for programs that screen thousands of women each year. Mammography was first introduced in the 1960's and has been the preferred method for the screening, diagnosis and treatment planning of breast cancer for the last thirty years.

There are a number of other imaging methods available, but the screen-film method is the most commonly used technique and is the only one applicable to this thesis.

A screen-film mammography machine usually comprises an x-ray source, a compression plate, a film plate and a grid that is placed between the patient and the film plate. The x-ray source is an x-ray tube made up of a cathode and an anode. The anode is made of molybdenum, a material that, when bombarded by photons, will emit electromagnetic energy in the form of x-rays. The x-ray tube is a vacuum tube with an electrical potential (i.e., voltage difference) that allows photons to be directed toward the target/anode/source (Figure 2.1).

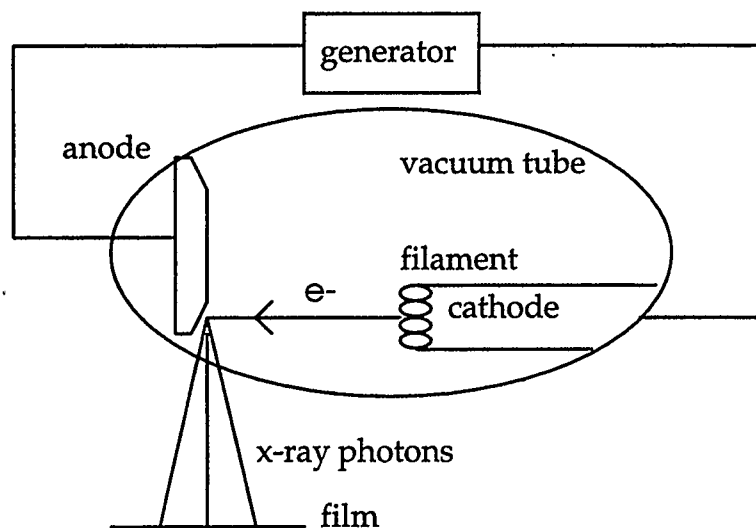


**Figure 2.1**

### **Detail of Anode and Cathode Configuration**

Once the x-rays have been produced, they are directed through the object (e.g. breast) which is compressed between the compression plate and the film plate, toward the film plate which holds a film cassette. The best film exposure is dependent on the time interval that the x-rays are released and directed toward the film.

The film, when exposed, will show the internal details in the breast. Calcifications are readily visible in films of breasts that are low density. The amount of detail that can be observed on the film is reduced with the increased density of the breast. The explanation for this can be found in Section 2.5. Lumps or tumours as well as veins can also be identified if the image contrast is high (i.e., the object being imaged is clearly visible against the surrounding

background) [Sprawls, 1977]. As with any imaging system, the quality of the film and equipment will determine the quality of the final product which, in this case, is the mammographic film.

The following diagram illustrates the components of a typical screen-film mammography device.

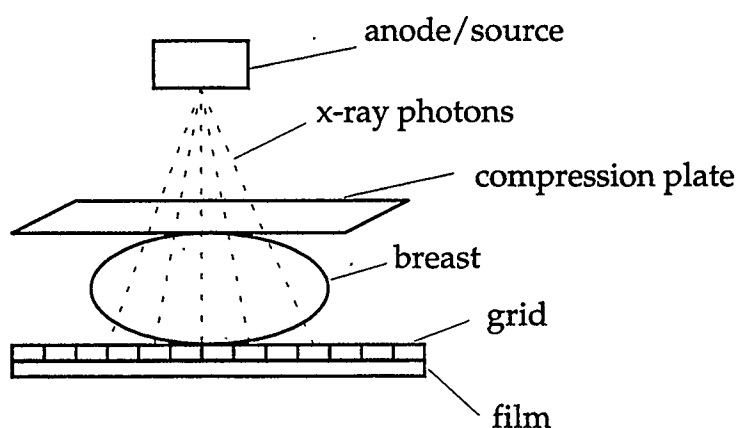


**Figure 2.2**

### **Components of a Typical Mammography Device**

This thesis is concerned with the detection and 3-dimensional reconstruction of calcifications and, therefore, a description of calcifications is included here. "Calcium is a silver-white bivalent metallic element of the alkaline-earth group. Calcification is the deposition of calcium salts in tissues. Calcification in the breast has been shown by spectrometric analysis to be in the form of calcium hydroxyapatite or tricalcium phosphate" [Bassett, 1992].

For this research, however, lead pellets are used in place of clinically diagnosed calcifications.

## 2.1 PHYSICS OF MAMMOGRAPHY

X-rays were discovered by German physicist W. K. Roentgen in 1895. Since 1901, x-ray imaging has been widely used as a basic tool in clinical medicine. X-rays are a form of electromagnetic energy that is similar to light waves or radio waves. Electromagnetic waves have wavelengths in the order of 100 nm (nanometres) to 0.01 nm whereas visible light wavelengths are in the order of 1000 nm. Electromagnetic waves can be described as having the properties of both waves and particles (e.g., they have a wavelength and frequency which are related by the equation  $f=1/\lambda$  where  $f$  is the frequency and  $\lambda$  is the wavelength). See Figure 2.3.

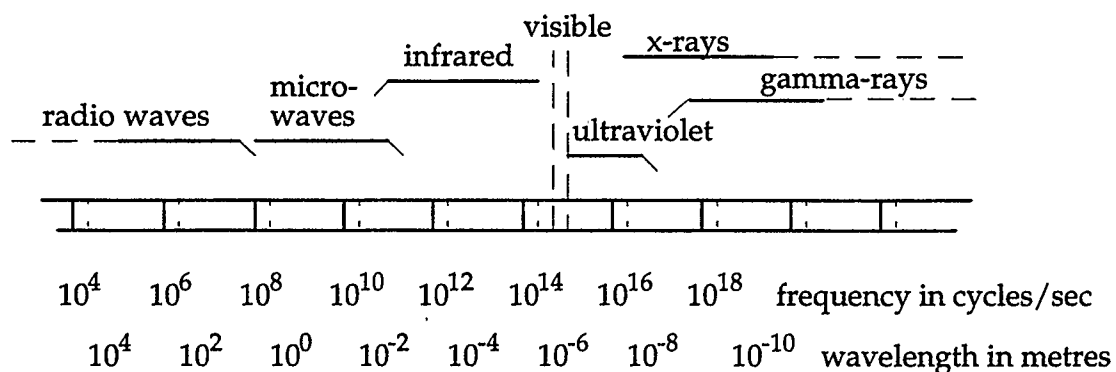


**Figure 2.3**

### Typical Wavelength and Frequency Ranges

(taken from Physical Science Study Committee, 1965)

The underlying physics of mammography determine the ability of the system to image the object and the ability of one to take advantage of the



The underlying physics of mammography determine the ability of the system to image the object and the ability of one to take advantage of the geometry to reconstruct the object. The understanding of the physics starts with the material of the anode and the voltage of the electrons that are used to bombard the target which is also known as the anode. For low-dose radiation, the electrons must bombard the target with “just enough” energy to give off x-rays which can reach the film. The results of mammography are affected by the amount of radiation used and the method of x-ray production.

The average x-ray dose for a complete mammogram (four views) is 0.17 rads or 170 millirads ( $1/1000 \text{ rad} = 1 \text{ millirad}$ ) [Zhou, 1989]. By comparison, a chest x-ray examination results in an x-ray dose of 10 to 20 millirads and a complete dental x-ray dose is 400 millirads. An extrapolation made by the technologists at Screen Test Alberta suggests that it would require 300 mammograms over ten years to increase the risk of breast cancer by 0.01%. This indicates the relative safety of implementing a screening program.

A short description of the methods of x-ray production that are applicable to mammography follows in the section on the physics of x-ray generation in Section 2.2.

Attenuation is another very important concept in the production of x-ray images. It is the decrease in the x-ray intensity due to the interaction of the photons with the material being imaged (i.e., bombarded by x-rays).

imaged via x-rays than others. Calcifications have much higher attenuation coefficients than tissues, so micro-calcifications can be identified on screen film mammograms. There is a linear-attenuation  $\beta$  coefficient and a mass-attenuation coefficient  $\beta/\eta$ . The following equation shows the contribution of each of the effects due to x-ray generation. These effects are discussed in Section 2.2.

$$\beta = \beta_{\text{coherent}} + \beta_{\text{photoelectric}} + \beta_{\text{compton}} \quad (2.1)$$

where:

$\beta$  is the linear-attenuation, the sum of the attenuation due to the various interactions.

$\beta_{\text{coherent}}$  is the attenuation due to coherent scattering

$\beta_{\text{photoelectric}}$  is the attenuation due to the photoelectric effect

$\beta_{\text{compton}}$  is the attenuation due to Compton scattering

The mass attenuation coefficient is found by dividing the linear attenuation coefficient ( $\beta$ ) by the mass of the material ( $\eta$ ).

A graph indicating the relation between the mass attenuation coefficient and the photon energy of a few materials is demonstrated in Figure 2.4.

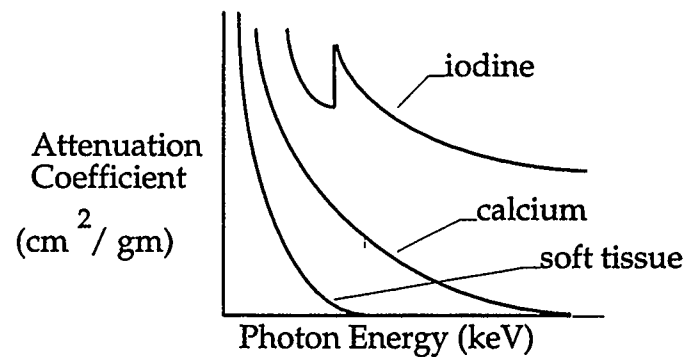


**Figure 2.4**

### **Attenuation Coefficient versus X-ray Photon Energy**

Some examples of mass attenuation coefficients [Sprawls, 1977] in  $\text{cm}^2/\text{gm}$  at 30keV x-ray photon energy are:

soft tissue:	0.4 $\text{cm}^2/\text{gm}$
calcium:	8.0 $\text{cm}^2/\text{gm}$
lead:	30 $\text{cm}^2/\text{gm}$

The factors that are related to the attenuation properties of a material are the photon energy, the atomic number, the density of the object, the electron density and the material's thickness.

The anode size and material also affect the production of the image. The geometry for the three-dimensional object reconstruction is determined by the physics of the radiation and the geometry of the x-ray source with respect to the film plate.

## 2.2 PHYSICS OF X-RAY GENERATION

X-rays are generated by high-energy electrons striking a target of tungsten or molybdenum. There are a number of different effects depending on the energy of the electrons and the atomic number of the target material. The production of white radiation, characteristic radiation and auger electrons are some of these effects.

White radiation (Bremsstrahlung) is produced when high-energy electrons interact with the nuclei of the tungsten atoms. If the high-energy electrons interact with the orbital electrons, characteristic radiation is produced. X-ray radiation is an ionising radiation meaning that electrons can be knocked out of the orbit around the molecule by the incident electrons. X-rays that are used in diagnostic tools interact with the orbital electrons causing less radiation to be emitted. The x-ray photons must be much higher in energy to interact with the nuclei.

Interaction between the x-rays and the atoms or molecules in matter (in the case of mammography it is a molybdenum target) can be classified in five different ways.

1. Coherent scattering
2. Photoelectric effect
3. Compton scattering
4. Pair production
5. Photodisintegration

Coherent scattering occurs during low-energy radiation when a photon (high energy electron also defined as a quantum of energy [Sprawls, 1977]) collides with another particle and is deflected in another direction without losing much energy. With little or no change to the photon's energy, there is an insignificant change to its wavelength. Because there is not enough energy to eject the orbital electrons from their orbit, coherent scattering does not cause ionisation.

The photoelectric effect occurs when an incident x-ray, with a slightly higher energy than that of the binding energy of a K-shell electron (the shell closest to the nucleus), collides with an orbital electron and ejects it from the orbit. This ejected electron becomes a photoelectron. The incident photon gives up all of its energy.

The photoelectric effect is the preferred form of interaction in x-ray imaging because the incident x-ray photon is completely absorbed thus reducing scattered radiation. This is desirable because scattered radiation is a health risk to equipment operators and it contributes to the noise on the films making them harder to interpret.

Compton scattering is similar to the photoelectric effect except that only part of the energy of the photon is transmitted to the electron. This means that the photon is scattered in other directions by the electron and the photon is reduced in energy (i.e., the wavelength increases). Compton scattering is

undesirable in x-ray radiography because of the noise that it produces on the films and the health hazard it creates for the personnel using the equipment.

Pair production and photodisintegration are interactions that involve the nucleus and require very-high-energy incident photons. These are of little interest in x-ray radiography and mammography because of the high radiation levels created. Therefore, they will not be described in this thesis.

In summary, the photoelectric effect and Compton scattering are the most common forms of interaction encountered in diagnostic x-ray radiography and always occur in some combination. The photoelectric effect is the most desirable interaction for imaging and the Compton scattering is the least desirable due to the noise it creates on the films. The goal is to increase the photoelectric effect and reduce the Compton scattering.

### **2.2.1 COMPONENTS OF AN X-RAY TUBE**

The x-ray tube produces the x-rays that are used in diagnostic imaging. The materials used for the target/anode and the voltage potential between the electrodes (i.e., anode and cathode), also known as the tube voltage, determine the type of radiation to be generated.

The materials most commonly used for the anode in a diagnostic radiology machine are tungsten and molybdenum. Molybdenum is the most common anode material in mammographic machines.

The cathode of the x-ray tube is made up of two elements, a tungsten filament and a metallic focusing cup which is used to focus the electrons that are emitted by the filament. The electrons produced at the cathode are accelerated toward the anode by applying a high voltage potential.

To create the high voltage potential in the x-ray tube that is needed to accelerate the photons toward the target/anode, a constant-potential, high-frequency, inverter-type generator is used. Tube voltage can consist of alternating current or direct current but full-wave or half-wave rectification is necessary to guarantee a constant potential. Details of the generators that are used may be found in Barnes, [1991].

Typically, the electrodes of the x-ray tube are sealed in a vacuum. This allows for better control of the number and speed of electrons that strike the anode.

There is a window tube-port through which the x-rays are directed before they reach the object and film. A beryllium window tube-port is used to limit the amount of scattered x-rays from the source. The anode is tilted so that the x-rays are directed through the port toward the object to be imaged.

The effective x-ray tube angle is the angle between the chest wall, which is perpendicular to the film plane, and the surface of the x-ray tube target (see Figure 2.5).

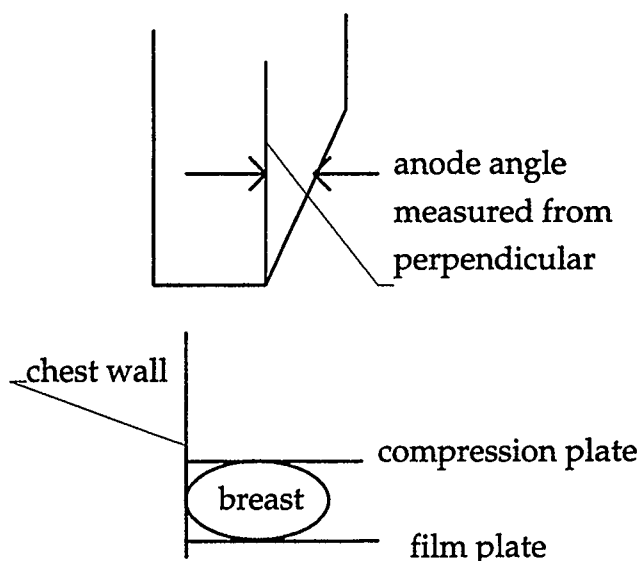


**Figure 2.5**

### **Anode Angle**

This angle is adjusted to allow coverage of the different film cassette sizes. As an example, if the SID (source-to-image distance) is 60 centimetres, and the cassette being used is 24 cm by 30 cm, for 24 cm coverage, an effective target angle of 22 degrees is required. This can be achieved by using a tube with a 22 degree angle or by using a tube with a lesser tube angle and by applying a tilt to the anode (i.e., tube tilt of 6 degrees and target tube angle of 16 degrees).

A generator is needed to create the x-rays. The industry standard has become the high-frequency, inverter-type generator that ensures a constant potential and, therefore, a more reliable and even film development. The generator is attached to the x-ray tube where the generated electrons are directed towards a rotating molybdenum anode. The target is set at 16 degrees and the



tube is set at an angle of 6 degrees for an effective target angle of 22 degrees which has been found to be the optimum target angle for mammography [Long, 1991]. This angle results in the maximum effective focal spot size.

### 2.2.2 GEOMETRY OF X-RAY SOURCE

Better images are generated when a smaller focal spot is used. However, a larger anode angle allows for a larger bombardment area (i.e., more efficient x-ray generation) which increases the heat build-up.

The focal spot (source) is the effective anode size. A large anode affords a larger area for bombardment resulting in more x-rays being produced and less concern about overheating of the anode. However, a larger anode also means that a larger focal spot would be utilised and would result in the production of poorer quality images. For optimum image quality, the smallest possible focal spot is desired. Therefore, the anode is tilted at an angle of between 5 and 15 degrees to change the effective anode size and it is rotated to allow it to cool by constantly changing the area being bombarded by the electrons.

The following equation relates the effective focal size to the length of the actual focal size of the anode.

$$f = F \sin \theta \quad (2.2)$$

where

- $\theta$  is the anode angle

- $f$  is the effective focal size
- $F$  is the actual focal size

The distribution of the intensity of the x-rays during the acquisition of an x-ray image is referred to as the heel effect. The x ray intensity is lowest on the anode side at 30%, increases to 100% at the central ray and then tapers off slightly to 95% at the cathode side [Sprawls, 1977]. The heel effect is due to a non-uniform intensity distribution of x-rays leaving the x-ray tube (Figure 2.6).

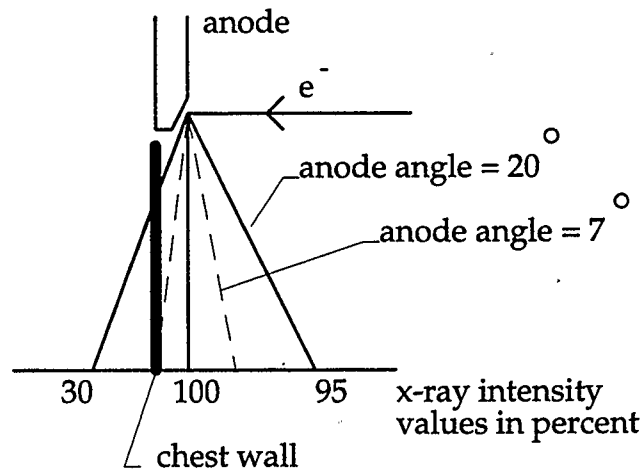


**Figure 2.6**

### Diagram of Heel Effect

Adjusting the anode angle is one method for improving the images. Another method is to reduce the noise due to scattered x-rays. The most effective way of reducing the noise is to use a grid made up of a series of lead foil strips which are separated by x-ray transparent spacers. The grid blocks the scattered radiation and allows the primary radiation to pass through. However,

when a grid is used, a longer exposure time is needed which increases the patient's risk. The improved images outweigh the patient's risk due to increased exposure and, in general, a grid is utilised. For this thesis, a grid was not used due to the configuration of the special adaptation equipment (i.e., a film table as described in Chapter 5) which was constructed to emulate the required stereotactic attachment.

### **2.3 MAMMOGRAPHIC EQUIPMENT**

The screen-film mammography device used for this thesis was a LORAD M-III Breast Imaging System. The LORAD M-III system is the primary mammography machine at Screen Test Alberta. Some of the important aspects of this machine include the x-ray tube specifications with respect to the anode material. The anode of the LORAD M-III is a rotating molybdenum target. The focal spot size can be adjusted from 0.1 mm or 0.3 mm. For this thesis, the 0.3 mm focal spot size was used so that the whole film cassette would be exposed. The target/tube angle is used to adjust the effective focal spot. In the LORAD M-III mammography machine, the target/tube angle range is between 4 and 16 degrees.

The assembly of the source and the film plate can be rotated through angles of +185/-165 degrees in the X-Z plane (see Figure 2.7) The source-to-image distance (SID) is 65 cm when the Bucky grid is used and the magnification

is approximately 1.8 times. A Bucky grid is a reciprocating (oscillating) grid that reduces scattering of the x-rays and focuses them toward the film. There are many different grids available and they all are used to focus the x-rays toward the film. A typical strip density is 30 to 50 lines per centimetre. A grid ratio of 4:1 or 5:1 is common. This ratio is determined by taking the ratio of the grid height to the interspace width. The higher the grid ratio, the more efficient is the grid in controlling scatter. However, a higher dose of radiation is required for the higher ratio grids and therefore they are not generally used.

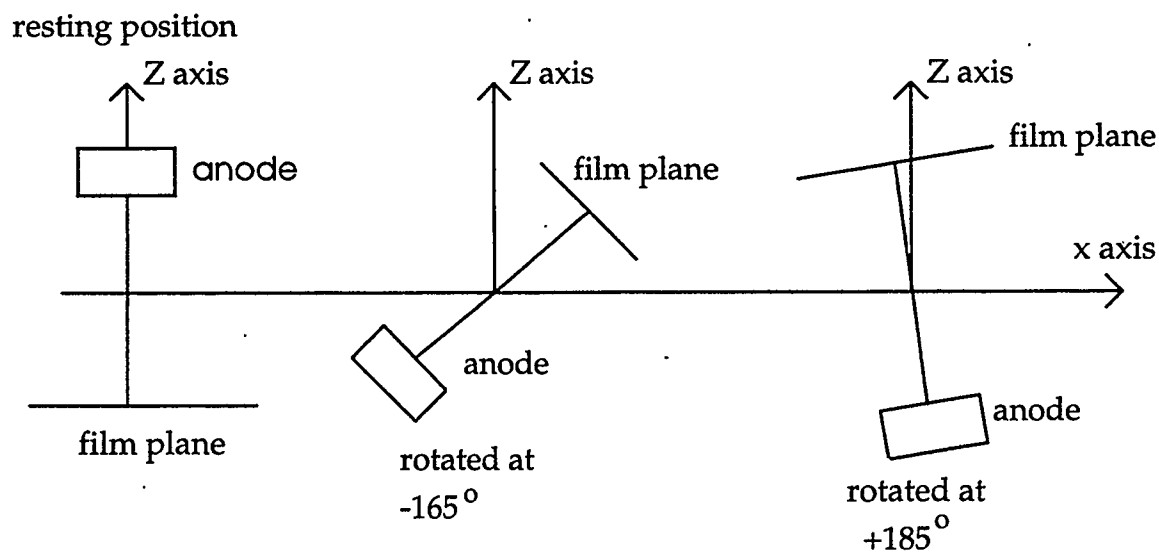


Figure 2.7

### Assembly of Source/Anode and Film Plane

The film used by Screen Test is a single sided double-emulsion film with a spatial resolution better than 0.1 mm supplied by Dupont (Dupont Cronex Microvision C Fast Detail film, Dupont Canada Medical and Imaging Systems,

Calgary, Canada). Low dose radiation in the order of 150 millirads is sufficient to cause exposure of these films.

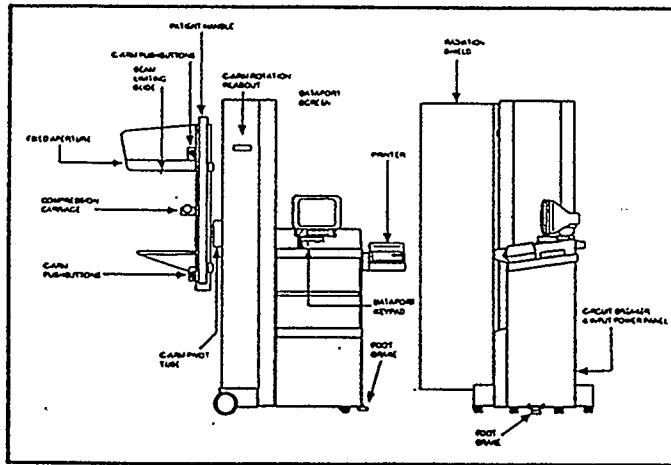


Figure 2.8

### LORAD M-III SYSTEM

(taken from the LORAD M-III Operating Manual)

#### 2.4 BREAST CANCER FEATURES VISIBLE ON MAMMOGRAMS

Breast cancer can present itself in many different forms. In some cases, there are cysts/tumours or masses, and in others, there are calcifications, (large: benign, small and in clusters: malignant). Both of these features can be found on the mammogram. A tumour, which is a mass with volume, can be seen as a poorly-defined shadow in the mammogram. However, in some cases, the breast is so dense that a mass cannot be identified.

In the case of calcifications, the mammogram usually gives a good image if the breast is not too dense. Even microcalcifications can be seen on mammograms. This is due to the position of the film with respect to the breast that is being imaged. With the breast between the x-ray source and the film, the image is magnified slightly making the smaller features more visible.

The calcifications can be as small as a pinpoint on the developed film or as large as a few centimetres. The size, shape and number of the calcifications is an indication of their status (i.e., benign or malignant). If they are large, alone and have smooth edges, they are usually benign. If the calcifications are tiny, occur in clusters and have rough edges, they are usually malignant [Shen, 1993]. There are many traits that the radiologists look for when viewing mammograms and the calcifications are primary indicators as to the existence of breast cancer [Sickles, 1986].

With the current methods of mammography, only two views are obtained. They are usually at about 90 degrees to each other. The two views are the cranio caudad view and the medio-lateral oblique view [see Figure 2.9]. The value of the angle is not exactly known.

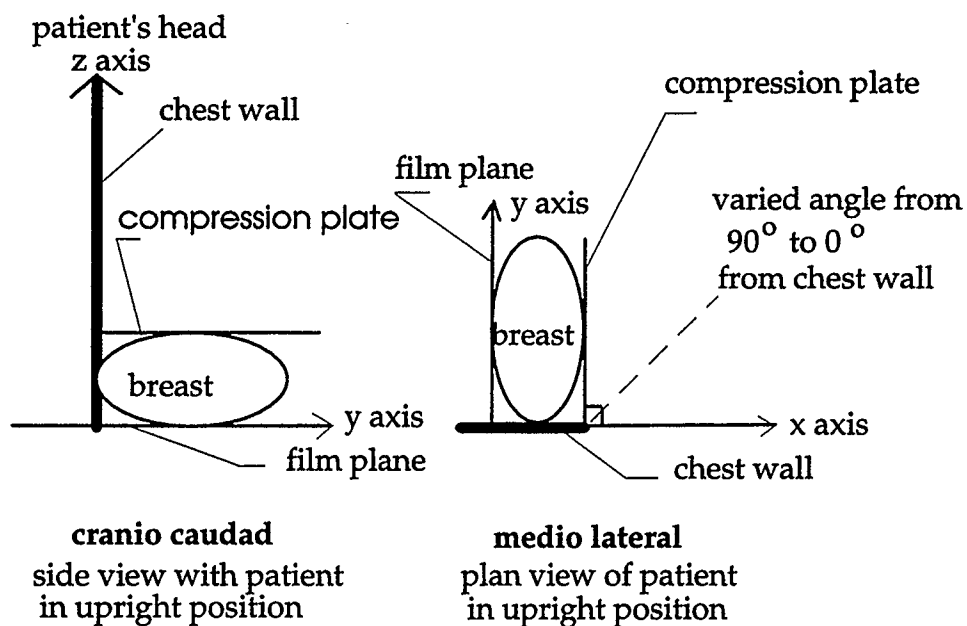


Figure 2.9

### Cranio Caudad and Medio-Lateral Views

The radiologist must rely on experience to interpret the two dimensional images and estimate the locations of any calcifications. The compression of the breast causes deformation so that when the breast is compressed in one direction for one film and subsequently compressed at approximately ninety degrees for the other film, the ability to locate features becomes very difficult.

Some calcifications are so tiny that only a very experienced radiologist and high-quality films make their detection possible. In some cases, the microcalcifications are overlapping each other such that portions of some calcifications are partially occluded causing them to appear to have very rough edges. This may result in a false positive diagnosis. In other cases, some of the

calcifications are completely occluded and a false negative diagnosis is possible [Shen, 1993].

Potentially malignant microcalcifications occur in clusters of fifteen or more, have rough edges, and resemble a moving train. A cluster of fewer than ten with smooth edges which look like they belong and do not appear to be on-the-move are most likely benign. This does not preclude the possibility that they might become malignant at a later date. "Calcifications occur in both malignant and benign disease of the breast" [Franceschi et al, 1990].

"The presence of linear or branching patterns, clusters of more than 15 and small microcalcifications have a higher probability of cancer" [Franceschi et al, 1990].

The above mentioned features of calcifications, clusters of microcalcifications and cysts are just a few of the indications that are visible on screen film mammograms. The clusters of microcalcifications have been identified as a primary indicator of breast cancer [Shen, Rangayyan, Desautels, 1992] and are, therefore, the indicators that were chosen to be modelled for this research. In most cases, the microcalcifications are in the order of a few microns. This size of microcalcification was considered to be too small to model as a first attempt so 1.0 mm diameter lead pellets were chosen as the physical model of the calcifications. Lead pellets of 1.0 mm diameter are typically used in breast



cancer screening for indicating moles or other landmarks on the exterior of the breast. This size of calcification is easily seen on screen film mammograms.

## 2.5 REQUIREMENTS FOR QUALITY IMAGES

There are six basic requirements for a good mammography facility. This ensures quality mammograms and patient safety [Long, 1990].

The requirements are:

- Dedicated mammography unit
- Specific mammographic film screen combination
- Dedicated film-processor
- Specially-trained technologist
- Radiologist with special interest in mammography
- Continuous quality control

The research work for this thesis was done with the Screen Test, Alberta Program for the Early Detection of Breast Cancer in Calgary, Alberta. All of these requirements were met because Screen Test Alberta is one of the 22 mammographic clinics in Alberta that has been fully accredited using the above requirements. All mammograms for this thesis were performed by the same qualified technician, thereby minimising any inter-tester errors and ensuring a high quality, consistent standard of image.

Once the above requirements have been met, the next consideration in the acquisition of quality images is the film. There have been improvements made to the radiation levels used in mammography in the past decades as well as to the manufacture of the films. This has improved the resolution and contrast properties of the developed image.

There are a number of factors that affect the radiographic resolution [Long, 1990]) and they include:

**Motion unsharpness due to:**

Immobilisation (compression)

Exposure time

Patient preparation

**Geometric unsharpness due to:**

Focal spot size

Focal-Object distance

Object receptor distance

**Receptor Unsharpness due to:**

Screen characteristics

Film characteristics

Optimal mammographic depiction of breast calcifications requires:

- Taut compression of the breast to decrease its thickness and reduce scatter radiation and motion.

- High output x-ray tube with a molybdenum target operated at a low peak kilovoltage setting, usually 26-27 kV to maximise the photoelectric effect.
- Reciprocating grid to image dense or thick breasts.
- High-contrast film.
- Optimal processing of the film - including extended development time for appropriate single-emulsion films.

Again, all of these requirements were met at Screen Test Alberta.

## CHAPTER THREE

### X-RAY PHOTOGRAMMETRY

X-ray photogrammetry has been used for many applications over the last 30 years. The applications have ranged from orthopaedics to industrial materials failure research. However, in the field of mammography, the photographs or screen-films have been used for qualitative interpretation purposes rather than for gathering metric information.

Photogrammetry is defined as the technique of making measurements on photographs to determine geometrical data in the form of size, position and shape of photographed objects. The basic geometrical property of x-ray photographs or radiographs is the central projection. This is also true of ordinary photographs [Hallert, 1970].

This thesis proposes to use x-ray photogrammetry to remove the ambiguity of overlapping calcifications by reconstructing a three-dimensional object (i.e., the breast with calcifications) and giving unique three-dimensional co-ordinates to the features (in this case, lead pellets in a Plexiglas phantom representing calcifications) in the breast.

The basics of x-ray photogrammetry will be reviewed and its relation to mammography will be explained. The benefits of stereo viewing in mammography will also be discussed.

### 3.1 PRINCIPLES OF X-RAY PHOTOGRAMMETRY

Only the principles of photogrammetry and x-ray photogrammetry that are directly related to this thesis, specifically, the method of image creation and object reconstruction, will be discussed.

X-ray photogrammetry is similar to visible light photogrammetry in many ways. Therefore, it will be discussed in terms of visible light photogrammetry and the significant differences will be indicated.

Photogrammetry uses visible light to form images on a photographic emulsion film. Visible light is a form of electromagnetic radiation that has a relatively long wavelength of about  $10^{-6}$  m. This electromagnetic radiation is radiated or reflected from the object to a collector and focused onto a receptor to form an image.

The x-rays behave the same as light rays and conform to the same laws of physics. Because the wavelength of x-rays is 10,000 times shorter than the visible light wavelength, it is easier for the waves to penetrate matter. Visible light waves have a long enough wavelength that that they are absorbed or reflected rather than allowed to pass through an object. As x-rays penetrate a material, some of the energy is lost and the intensity is reduced. This is called attenuation and was discussed in Chapter 2. Different materials have different attenuation factors and indicate the ability of x-rays to pass through them. In x-ray

photogrammetry, the energy emanates from a relatively small source through the object onto a receptor [McNeil, 1966].

On x-ray films, if the attenuation factor for a certain material is high, no x-rays will pass through causing the film to stay undeveloped. If the attenuation factor is zero, all the x-rays pass through and the film comes out black or fully developed.

Due to the x-rays passing through the material being imaged instead of being reflected off the object, the film records what appears to be shadows of the object. Points that are imaged on the films do not appear as distinct points.

Geometrically, the central projection is where the points on an object are imaged on a photograph via straight lines that pass through a single common point in space called the perspective centre. "In x-ray photography, the perspective centre is the focus of the roentgen tube" [Hallert, 1970]. The focus is assumed to be a mathematical point without dimension. This of course is not true in reality and results in deviations from the ideal geometric arrangement.

"The accuracy of x-ray photogrammetry depends much upon the definition of the points of the object to be measured. Therefore, the problem of distinct identification of the details of the object in the photograph is very important for the success of the photogrammetric procedure" [Hallert, 1970]. In x-ray photogrammetry, the images are shadows of the object and, therefore, have fuzzy edges which are difficult to measure. A finer edge results in a better

definition of the point. Identification is also difficult in x-ray images. A labelling method that is recorded in the image is necessary for accurate identification. Photographs that use reflected light can use details of objects or features near the point of interest in the image to help in the identification of points.

For stereophotogrammetry, two photos or films with the image of the object are obtained. The procedure uses overlapping photos to reconstruct a three-dimensional geometrical object. Again, points in both images must be correctly identified to be successful in the reconstruction process.

The basic concepts of photogrammetry are applicable to x-ray photogrammetry. These concepts include the interior orientation, the relative orientation, and the absolute orientation. The last two may also be considered together as the exterior orientation.

The interior orientation defines the position of the perspective centre (focus) with respect to the image plane. The principal distance or the focal length (also known as the source-to-image distance (SID) in x-ray photography) is the perpendicular distance from the focus to the image plane. The position of the footprint of the perspective centre on the image plane is the principal point.

The main differences between x-ray photogrammetry and visible light photogrammetry is in the definition of the interior orientation. What is referred to as the focal length in visible light photogrammetry is defined by the source to

image distance or working distance in x-ray photogrammetry. The perspective centre in visible light photogrammetry is defined in x-ray photogrammetry as the source or focus which is the x-ray tube.

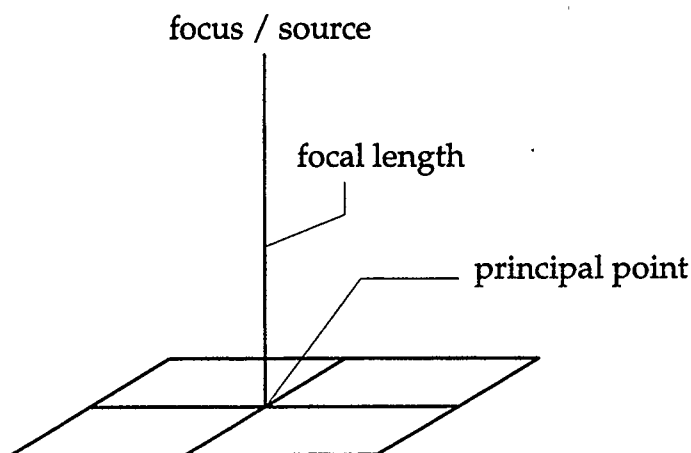


**Figure 3.1**

### **Diagram of Interior Orientation**

The complete interior orientation can be determined through calibration procedures. The calibration of the object and the system used in this thesis will be discussed in Chapter 4.0.

Relative orientation, in this case, analytical relative orientation, is the process of mathematically building a model of the object that has been imaged by stereo photographs (two photos that overlap and have common points that can be measured). There are two basic methods for analytical relative orientation. One method uses the coplanarity condition and the other uses the



collinearity condition. The basis of the collinearity condition is that the perspective centre, the image point and the object point all lie in a straight line.

Using the following equations, through similar triangles, if the perspective centre and the image coordinates are known, the three-dimensional position of the imaged object can be calculated.

$$x_a = -f \left( \frac{m_{11}(X_A - X_L) + m_{12}(Y_A - Y_L) + m_{13}(Z_A - Z_L)}{m_{31}(X_A - X_L) + m_{32}(Y_A - Y_L) + m_{33}(Z_A - Z_L)} \right) \quad (3.1)$$

$$y_a = -f \left( \frac{m_{21}(X_A - X_L) + m_{22}(Y_A - Y_L) + m_{23}(Z_A - Z_L)}{m_{31}(X_A - X_L) + m_{32}(Y_A - Y_L) + m_{33}(Z_A - Z_L)} \right) \quad (3.2)$$

Where

$X_A, Y_A, Z_A$  are the ground coordinates

$X_L, Y_L, Z_L$  are the coordinates of the perspective centre

$x_a, y_a$  are the image coordinates

$f$  is the focal length or, for this research the source to image distance

$m_{ij}$  are the elements of the rotation matrix

The coplanarity condition is the method that was used for this thesis and requires that the two sources, the image points of one point and the three-dimensional model point all lie in one plane.

The final object reconstruction is achieved by performing an absolute orientation. This takes the model coordinates that are calculated in the relative orientation and transforms them into the object coordinate system. This

orientation and transforms them into the object coordinate system. This procedure is merely a conformal transformation that maintains angles and relative distances. A seven parameter similarity transformation was used to obtain the final calculated object points of the reconstructed object.

The actual techniques, their application and results are detailed in Chapter 6.

### **3.2 APPLICATION OF X-RAY PHOTOGRAMMETRY TO MAMMOGRAPHY**

Mammography has traditionally used two films at 90 degrees to one another to acquire the maximum coverage of the breast. This is, and will be until other methods are more economical and more easily accessed, the best method of detecting early indications of breast cancer. However, if breast cancer is suspected and a clearer idea of the size and location are needed, stereo mammography allows for a better diagnosis and can also be used for treatment planning. Stereotactic mammography is used for biopsies and FNA (fine needle aspiration) techniques and biopsies. For the needle biopsy, the breast is held immobile by the compression used during the imaging process. The stereo images are used to establish the position of the cells that are to be removed. There are limitations due to the machine in that it can only view a portion of the breast that is 5 cm by 5 cm and the angle between the films is only approximate (within a few centimetres).

There is a stereomammography machine in Edmonton which uses digital images and can produce screen-films as well. This machine is used mostly for needle biopsies where cancer is suspected and a confirmation is needed. The demand for this service has been high and allows for minimal invasion. With the digital images, the operator must pick the conjugate points in the two images leading to potential errors.

X-ray photogrammetry has been successfully applied to many areas in medicine in the past. When imaging bones or very dense material with x-rays, a good image can be obtained. Mammography does not lend itself well to x-ray imaging unless there is a great deal of contrast and objects of different densities are present. For this research, however, calcifications and lead pellets show up well on the x-ray films and are distinct enough features that x-ray imaging is useful. These distinct features make the use of x-ray photogrammetry possible.

### **3.3 BENEFITS OF STEREO VIEWING IN MAMMOGRAPHY**

The benefits of stereo viewing in mammography cannot be emphasised enough. It has been proven that stereo viewing of any object improves the information that can be gained [Chelberg, 1994]. Along with a better appreciation of the size and shape, the location of points-of-interest is enhanced.

Depth perception is the primary benefit of stereo viewing. Monocular vision is detrimental to the understanding of objects. A photograph that is two-

dimensional can appear, for example, to have a bird sitting on a person's head when in fact the bird is sitting on a branch 10 feet behind the person. With depth perception, one perceives that the bird is behind the person. In photogrammetry, the actual position of the person and bird can be calculated. In mammography, a depth map of the details in the mammogram improves the conceptualisation of the location and size of the details.

X-ray photogrammetry if executed with care and with the existence of control points, can give a higher degree of accuracy and should minimise the invasiveness of any following procedure such as FNA (Fine Needle Aspiration) or mastectomy.

## CHAPTER FOUR

### PHANTOM CONSTRUCTION AND CALIBRATION

The construction and calibration of the object (phantom) that is imaged for this thesis is described in this chapter.

Phantoms for breast imaging machines do exist and are readily available. However, they are limited to a two dimensional plane which is unacceptable for the purpose of this research. Therefore, a new phantom was devised. In addition, it is necessary to calibrate the phantom for the purpose of error estimation and to improve the interpretation of the quality of the results.

In the construction of the phantom, the materials and the shape were chosen with careful attention to the concerns related to the techniques and concepts to be applied in this research.

This thesis depended on having an object that could be reconstructed from x-ray images obtained from a mammography machine. The requirements for this phantom included:

- repeated exposure to radiation
- representation of overlapping and non-overlapping calcifications
- base material must be transparent to x-rays (attenuation coefficient  $\sim 0$ )
- sturdy - little deformation due to heat and cold
- large enough that it could be measured by traditional survey methods
- small enough that it was a reasonable representation of a female breast

#### 4.1 CHOICE OF MATERIALS FOR A PHANTOM

The materials that were chosen for the phantom needed to create visually similar effects on the film to an image of a female breast that contains calcifications. The attenuation coefficients of the representation of the calcifications must be similar to the actual attenuation coefficients of calcifications in the breast. The rest of the phantom needed to be transparent to the x-rays to limit possible confusion between the objects of interest and the base structure.

Throughout the literature in x-ray photogrammetry, Plexiglas and lead pellets, or lead strips drilled with tiny holes, are used for calibration purposes. In this thesis, lead pellets are used to represent the calcifications. Plexiglas is an x-ray transparent material that was used to suspend the pellets in a three-dimensional configuration. Multiple layers of thin pieces of Plexiglas allowed the re-creation of overlapping calcifications by positioning pellets at similar X-Y locations on two or more layers (i.e., at different Z values).

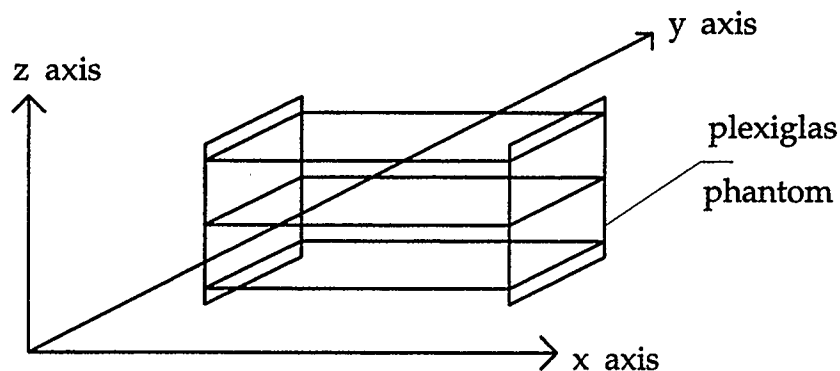


**Figure 4.1**

### **Diagram of Plexiglas Phantom**

The Plexiglas phantom is constructed so that the lead pellets are visible and easily reached so that survey and physical cube measurements between lead pellets were possible. The lead pellets that were used in the building of the phantom were the same ones that are regularly used in mammography as control points to help locate points of interest in the films. They were obtained from Screen Test Alberta. Each lead pellet is approximately 1.0 mm in diameter. A few were deformed slightly when they were embedded in the Plexiglas. This resulted in non-uniform diameters for the lead pellets and facilitated the identification of some of the points on the films.

#### **4.2 CHOICE OF SHAPE AND SIZE OF THE PHANTOM**

The shape and size of the phantom are important for the calibration procedure and the resemblance to the female breast makes the use of the mammography equipment practicable.

A square phantom was chosen to facilitate the calibration procedures and the placement of lead pellets to model the desired features of overlapping calcifications. Typical mammography phantoms used to calibrate the mammography machines are Plexiglas rectangle casings containing a layer of wax (~2.5 cm thick). The wax is embedded with various objects of different sizes, shapes and densities which represent different details that are visible in the mammograms. All of these are in one layer of the phantom making it a two-dimensional object and unacceptable for our purposes. Therefore, a new phantom was created.

In precision surveys, it is common to use an open metal frame cube of known dimensions with targets located on the frame. A theodolite is used to derive the coordinates of the targets/control points by means of solving a free network. Therefore, a cube was chosen as the preferred shape for the phantom.

The size of the phantom was dependent on the mammogram film size and was also influenced by the size of existing phantoms. The existing mammographic phantoms are all approximately 10 cm by 10 cm by 3 cm high representing a compressed breast.

In order to get the overlapping lead pellets placed correctly and accurately measure them with traditional survey techniques, it was necessary to increase the height of the phantom. Therefore, a 10 cm by 10 cm by 10 cm cube phantom was constructed with three levels of Plexiglas on which to place the



lead pellets. The additional height allowed each pellet to be sighted directly with the theodolite (i.e., not through the Plexiglas). If sighting of the pellets had been through the Plexiglas, bending of the light rays and distortion of the measured angle would have resulted. The increased phantom height also increases the variation in the Z values for the lead pellets.

### 4.3 MICROSURVEY OF PHANTOM

“Calibration is generally defined as the procedure of standardising (as a measuring instrument) by determining the deviation from the standard, so as to ascertain the proper correction factors. Calibrations are usually made under operational conditions because corrections have to be applied to measurements made under these conditions” [Hallert, 1970].

As mentioned earlier, the location of each of the lead pellets is needed to determine the quality (accuracy and precision) of the reconstruction techniques. Therefore, a microsurvey (due to the phantom’s size) was performed on the phantom.

The procedure for the microsurvey was as follows:

The phantom was placed on a stand in an empty room. Four theodolite stations were positioned around the phantom. One theodolite (WILD T2000) was set-up at station 101. From there, a second station was sighted as a backsight. The angles to the stations and the points on the cube were recorded.

There were tripods with prisms at each of the other three stations. To confirm the values computed from the theodolite measurements, the distance between each of the stations was measured with an uncalibrated cloth tape measure. Any scale error in the cloth tape will only cause a minor relative scale change. The elevations of each of the four stations were measured with a WILD level and rod.

A theodolite (WILD T2000) was set up at the first station 101 and station 102 was sighted. From this position, all the points visible from station 101 were sighted and their angles (face right) were measured. The instrument was transited (flipped over by  $180^\circ$  to face the opposite direction) and the station 102 sighted once more. All the points visible from station 101 were sighted again and their angles (face left) were measured. This was the procedure followed for all the stations 101, 102, 103 and 104 (Figure 4.2).

The lead pellets representing overlapping calcifications caused problems in the survey because of their close proximity to one another and the limitations of the theodolite and its angle measurements. Also, some of the pellets could only be seen from one station which limited the redundancy for the calculation of the coordinates. Due to limited time, only one set of measurements was taken that day.

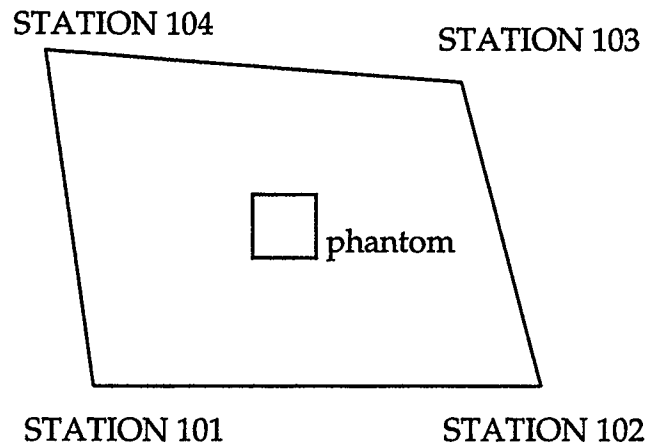


**Figure 4.2**

#### **Theodolite stations and phantom position**

The MONALYSA adjustment computer software was used to calculate the three dimensional coordinates of the phantom.

The input to the program included a number of measurements:

- The azimuth of each point sighted calculated in Microsoft EXCEL.
- The distance between pellets measured directly on the phantom with an engineering scale.
- The standard deviations for the angle and distance measurements.

The coordinates resulting from the MONALYSA program have been used as the ground control for the photogrammetric applications.

#### **4.4 ERROR ANALYSIS**

Measurements for this work included those made with a scale, a theodolite (WILD T2000), a level (WILD GM3), the WILD AC1 Stereo

Comparator for image coordinates and a cloth tape measure for the station locations. There are errors associated with each of these measuring instruments and these errors can be separated into different error categories.

All measurements are subject to errors which affect the quality of the measurement of the position of a point. Precision and accuracy are two concepts that describe the quality of the measurements. An understanding of the different types of errors is necessary for the determination of the accuracy and precision of the system in question. The potential sources of these will be reviewed.

First, the concepts of accuracy and precision will be defined and then the types of errors will be identified.

“Precision is defined as a quality associated with a class of measurements and refers to the closeness of repeated measurements about the mean ( in brief, closeness together) ” [Hallert, 1970].

“Accuracy is defined as a quality referring to the closeness of measurements, computations or estimates to the true values or values assumed to be true ( in brief, closeness to truth)” [Hallert, 1970].

The different types of errors that affect the accuracy and precision of any system of measurements are categorised as follows:

- gross errors or blunders
- systematic errors

- random errors

*Gross errors or blunders* are most commonly due to human error such as mislabelling, misreading a measurement or recording errors. Careful checking along with independent repetitions of measurements and careful attention to recording and measuring techniques are mandatory to avoid such errors.

*Systematic errors*, often called regular errors are due to biases in the measuring instruments and methods. Calibration of instruments such as a theodolite or level may reveal that certain readings are always off by part of a degree or 1 cm, respectively. If the bias can be determined, a correction can be applied. This form of error affects the accuracy of the measurements because it causes a deviation from the true value.

*Random errors* are small measurement errors that exist independently and are assumed to form a statistically normal or Gaussian distribution about a mean value. These errors are unavoidable but may be modelled statistically. Random errors affect the precision of the measurements.

Possible sources of blunders in this thesis are related to the mislabelling of the control points (lead pellets) of the phantom on the films. A labelling system was not developed before the phantom was imaged with the mammography machine. Therefore, when it came time to identify the images, a good understanding of the image acquisition geometry was necessary especially with respect to determining the overlapping points. Because some of the points are so

close together in the image, there is still a possibility of having a blunder remaining unnoticed.

The Wild T2000 theodolite reads angles to the nearest 0.1 seconds. In most cases, the horizontal angle measurements were different by 15 to 30 arc seconds of an angle measured between face right and face left.

The cloth tape was not calibrated for this application because it was used primarily as a check for the distances calculated from the angle measurements.

The Wild GM3 level was used only to assist in the determination of the elevation changes between the stations.

Standard deviations for the measurements were necessary for input into the MONALYSA network adjustment program. Initially, because of the precision of the theodolite of 0.1 seconds, the standard deviations were assumed to be small (i.e., 10 seconds). However, due to the nature of the MONALYSA program, much larger standard deviations were required to get the program to converge. MONALYSA allows only one value for the standard deviation for all of the readings from one station. Therefore, larger standard deviations for the measurements with poor redundancy (e.g. for pellets that could be seen from one station only) and smaller standard deviations for measurements with higher redundancy (e.g. for pellets visible from at least two stations) could not be accommodated. Horizontal angle standard deviations of between 200 and 600 arc seconds were used.

The estimated three-dimensional phantom coordinates were calculated using the MONALYSA program.

To have useful results, the errors inherent in the survey of the phantom must be understood and considered in the final analysis of the techniques used for this research.

The physical measurement of the phantom could be accomplished with a precision of 0.25 mm. This is the smallest value that could be measured with reasonable certainty. Systematic errors in the scale that was used for the distance between the lead pellets on the phantom is not known but the same scale was used for all the measurement so it should not affect the precision.

The films are single sided double emulsion photographic films. Sources of error for the films include the unflatness in the cassette at the time of exposure and stretching due to the film development process. Measurements made on the WILD AC1 Stereo Comparator include errors from mislabelled points and ambiguity due to the fuzziness of the edges of the imaged points.

The standard deviation associated with the measurements of the points on the films was estimated at 50 microns. However, when least squares methods were used to calculate the centres of the imaged points, this was found to be very pessimistic. The average standard deviation for the circles/points was between 2 and 30 microns.

#### 4.5 ESTIMATED PHANTOM COORDINATES

The estimated phantom coordinates and their associated positional errors (see Table 4.1) were found using MONALYSA, a network adjustment software package written by Zoltan Biacs of the Geomatics Department at The University of Calgary.

These coordinates have been transformed from the survey coordinates system to the coordinates system on the phantom itself. The estimated phantom coordinates are assumed to be without error for the purposes of the calculations executed in the next chapters.



Table 4.1

## Final Control Point Coordinates

POINT	X (mm)	Y (mm)	Z (mm)	X Error (mm)	Y Error (mm)	Z Error (mm)	Error Vector (mm)
1	0.00	0.00	0.00	0.0	-1.0	1.0	1.4
2	0.78	48.30	-4.17	0.0	0.0	1.0	1.0
3	0.42	96.05	2.30	0.0	0.0	1.0	1.0
4	48.31	47.51	-5.01	0.0	0.0	1.0	1.0
5	96.73	0.00	0.00	0.0	-1.0	1.0	1.4
6	96.25	48.87	-6.13	0.0	0.0	1.0	1.0
7	96.67	95.46	1.42	0.0	0.0	1.0	1.0
8	98.92	95.78	-2.97	0.0	-1.0	0.0	1.0
9	98.67	-0.57	-2.68	1.0	1.0	1.0	1.7
10	97.27	-0.00	-97.01	1.0	0.0	1.0	1.4
11	97.51	94.87	-97.05	0.0	0.0	1.0	1.0
12	95.71	47.92	-8.35	1.0	0.0	0.0	1.0
13	95.39	48.17	-51.11	1.0	0.0	1.0	1.4
14	95.53	47.93	-48.61	0.0	0.0	1.0	1.0
15	0.78	48.05	-47.44	0.0	0.0	1.0	1.0
16	0.41	48.05	-90.19	0.0	0.0	1.0	1.0
17	0.72	48.54	-6.54	0.0	0.0	1.0	1.0
18	0.40	48.54	-49.65	0.0	0.0	1.0	1.0
19	-0.16	47.54	-92.27	1.0	1.0	1.0	1.0
20	-2.83	96.10	-94.64	0.0	0.0	1.0	1.0
21	-1.83	96.48	-0.75	0.0	0.0	1.0	1.0
22	-3.14	0.30	-95.55	0.0	0.0	1.0	1.0
23	47.83	47.48	-93.06	1.0	1.0	1.0	1.7
			RMS	0.5	0.5	0.98	1.2

## CHAPTER FIVE

### STEREOMAMMOGRAPHIC IMAGING OF PHANTOM

The phantom was imaged using the mammographic machine at Screen Test Alberta. Stereo images were required for the three-dimensional reconstruction of the phantom. The system as it exists today was lacking the \$70,000 attachment necessary for obtaining stereo images. Therefore, the system was modified for this thesis.

#### 5.1 STEREO-IMAGING METHODOLOGY

To acquire stereo images, the gantry was rotated 15 degrees about the y-axis in the positive and negative directions with respect to the object which was set on a specially constructed film table. The film table consisted of a wooden stand with a Plexiglas slot for the film. Three films were taken, one at 0 degrees from the vertical (perpendicular to the film plane), +15 degrees from the vertical in the X-Z plane and -15 degrees from the vertical in the X-Z plane (see Figure 5.1). Kodak one sided double emulsion film was used for all of the images.

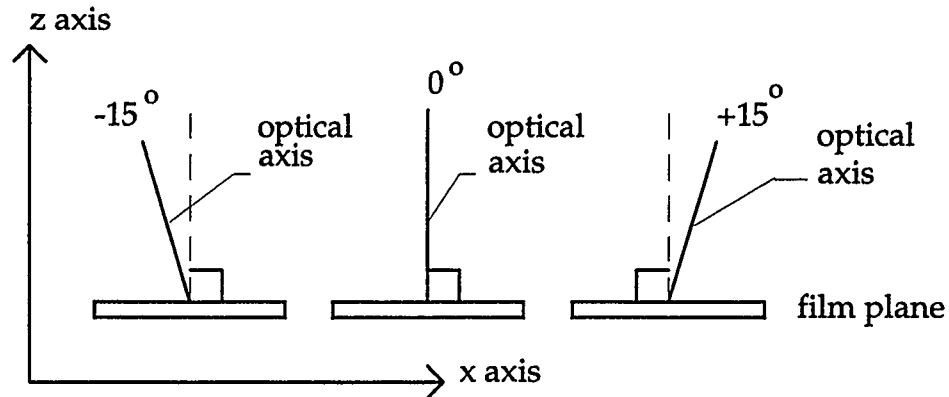


**Figure 5.1**

### **Film Acquisition Configuration**

Traditional stereo x-ray techniques use the 15 degree angle but also include a shift of the film so that the two exposures do not overlap. This method is open to human error and, therefore, is not desirable for precise photogrammetric applications.

## **5.2 FILM AND OTHER CONSIDERATIONS**

The film is important because the quality of the data relies on the sharpness of the edges in the image. Errors due to the unflatness of the film in the form of radial distortion should be considered and modelled if they are deemed to be significant. The method by which the film is developed is the primary cause of unflatness errors. Therefore, an understanding of how the film acquires the image and the method by which it is developed is also important in the determination of the salient errors. However, in general, the errors caused

by the film development are very small (in the order of 50 microns [ASP, 1980]) when compared to the errors caused by human errors during measurement acquisition.

### 5.3 ORIENTATION OF THE PHANTOM

The orientation of the phantom on the table holding the film was important in the determination of the corresponding points in the image and on the phantom. It was situated so that the lead pellets representing the calcifications overlapped. In retrospect, it would have been useful to initially situate the phantom so that all the points could be easily identified.

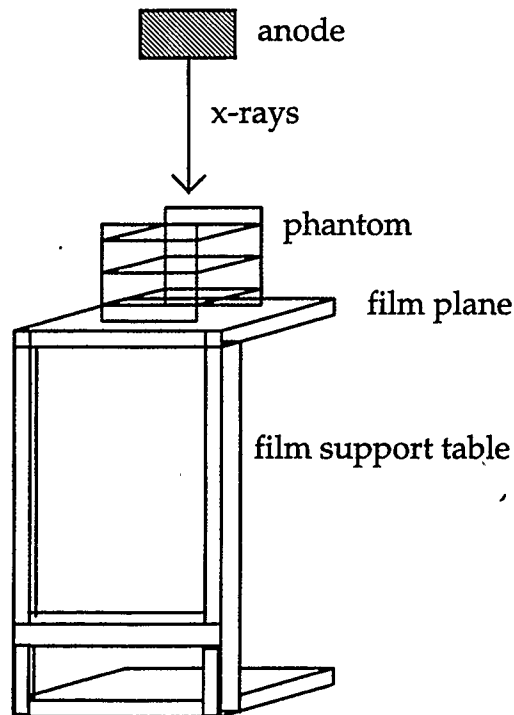


**Figure 5.2**  
**Phantom on Film Table**

#### 5.4 COORDINATE DETERMINATION OF PELLETS ON IMAGES

The images/films were digitised on the WILD AC1 Stereo Comparator in the mono comparator mode. This machine records the x and y coordinates of the targeted points. The 40 micron diameter circle of the pointing device was employed. Therefore, it was assumed that the best precision possible was greater than half of the diameter of the pointer circle or a minimum of 20 microns. It was found that the standard deviation of the measurements were between 2 and 30 microns. The fuzzy edges of the images affected the precision of the measurements made on the AC1 Stereo Comparator.

The films were placed in the comparator and each circle (shadow of the lead pellet) was digitised at the four quadrants (approximately) of each circle. In some cases, the circles overlapped and points at positions other than the quadrants had to be used. The centres of each of the circles were digitised and later used as the first approximation for the calculation of the centres of the circles.

Repeated measurements were not made because of the poor image definition as compared to the high precision of the WILD AC1 Stereo Comparator. Repeat measurements must be within 15 microns of the original measurement for them to be considered as the same point, otherwise that measurement is taken as a new point. The fuzziness of the imaged circles made it very difficult to obtain repeat measurements within the 15 microns. It was

possible to measure more points on the circumference of the circles but the extra time for an improved precision of a few microns did not seem appropriate. The films were placed in the comparator emulsion side up, similarly to the way aerial diapositives would be placed.

### **5.5 RESOLUTION OF THE IMAGES**

The films shown below can be measured to the nearest 2 to 30 microns using the Wild AC1 Stereo Comparator. Some of the features on a circle were clearer than others making the 2 micron precision possible.

## CHAPTER SIX

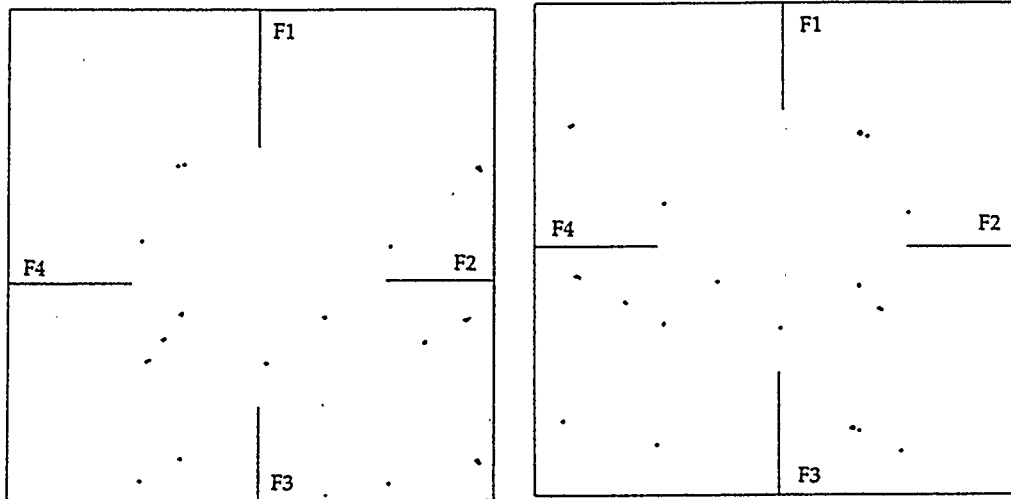
### OBJECT RECONSTRUCTION

This chapter will cover the geometric, physical and mathematical concepts utilised in the reconstruction process of a three-dimensional object. These include the geometry of the x-ray rays, the interior and exterior orientation, the geometry of the image acquisition machine and the mathematical models needed to complete the reconstruction analytically. This is an attractive method because of the geometry of the imaging set-up.

#### 6.1 APPLICATION OF X-RAY PHOTOGRAMMETRY TO OBJECT RECONSTRUCTION

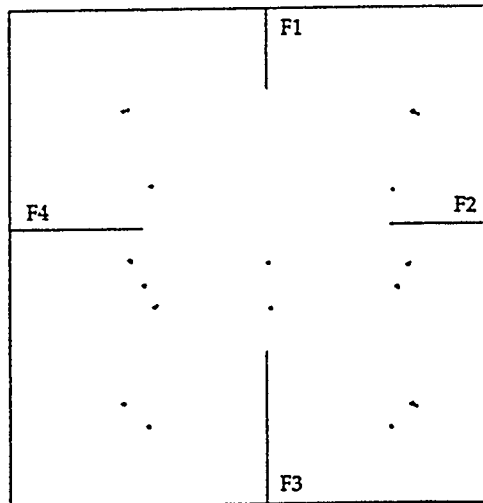
The application of x-ray photogrammetry to object reconstruction differs from regular photogrammetry primarily in the method of image creation. The remaining principles will be directly applied as if the images were acquired with visible light imaging techniques. Visible light images are created via reflected light waves from an object and x-ray images are created via x-rays passing through the object onto the film leaving a type of shadow on the film. For this research, only the lead pellets leave a shadow on the film leaving the majority of the film exposed with no features. This means that there is less information available for the reconstruction. The shading or texture in the x-ray images in this particular case is difficult to detect. For clinical mammograms, more detail

is available but there are no control points or fiducial marks. The following diagrams illustrate the limited information available in mammograms and in particular the films used for this thesis.



(a) Left Film

(b) Right Film



F1,F2,F3,F4  
Fiducial Marks

(c) Middle Film

Figure 6.1

Diagrams of Phantom Features on Films



To understand the accuracy and precision of this work, it is necessary to know the magnitude of the errors associated with the imaging techniques that were used. The images were measured on the AC1 Wild Stereo Comparator which has a precision of 1 micron. However, the precision with which I was able to make the measurements was closer to 30 microns. The phantom was surveyed with a precision of 1.0 mm. With these measurement capabilities, an object reconstructed by analytical photogrammetric techniques should be within 1 mm or 1000 microns. This is still better than what is possible with the mammographic methods currently being used for diagnosis and treatment planning where precision of 1 cm is possible.

To appreciate the magnitude of potential image measurement errors from, a calculation of the error associated with the imaging of a 1.0 mm diameter lead pellet is included here. The lead pellets, which are assumed to be 1.0 mm diameter spheres, are presumed to be imaged as circles instead of ellipses. The error associated with the assumption of a circle representation instead of an ellipse for the lead pellets can be determined [McNeil, 1966]. The following calculation shows that the centre of the circle is in error by  $\Delta x$  microns versus the centre of the ellipse.

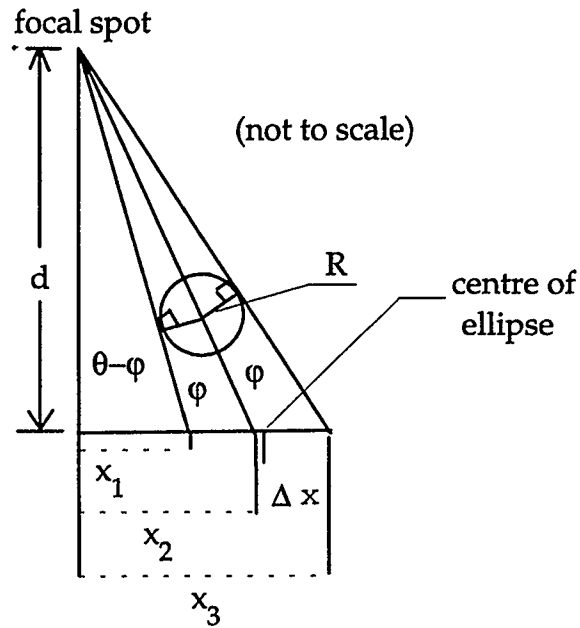


Figure 6.2

### Centre of ellipse versus centre of circle

$$\Delta x = \frac{d}{2} [\tan(\theta - \varphi) + \tan(\theta + \varphi) - 2 \tan \theta] \quad (6.1)$$

$d = 54 \text{ cm} = \text{source to image distance}$

$x_2 = 10 \text{ cm} = \text{distance from nadir point to centre of circle which is located at the centre of the film}$

$$\tan \theta = \frac{10}{54} \quad \theta = 0.1831108 \text{ radians} \quad (6.2)$$

$$\tan \varphi = \frac{0.05}{54} \quad \varphi = 0.0009259 \text{ radians} \quad (6.3)$$

For a lead pellet with diameter of 1 mm, the radius of the pellet is 0.5 mm or 500 microns.

$$\begin{aligned}\Delta x &= \frac{54}{2} [\tan(0.1831108 - 0.0009259) + \tan(0.1831108 + 0.0009259) - 2 \tan(0.1831108)] \\ &= 0.0932 \text{ microns}\end{aligned}$$

An error of 0.09 microns is 0.009% of the total diameter of the actual pellet which shows that the error associated with using a mathematical model of a circle for the lead pellets instead of an ellipse is acceptable for the level of accuracy and precision that is required for this research. Because the edges of the image of the lead pellet is a shadow and not a definite line, larger errors than those associated with the math model will be more likely to occur due to human error in the digitisation of the edges with the Wild AC1 Stereo Comparator (up to 30 microns as explained in Chapter 5).

True three-dimensional information is not available with x-ray imaging unless multiple images are acquired. The benefit of stereo mammograms is that the information from stereo images is still greater than if the traditional unrelated two-dimensional images are used and the radiation dosage remains unchanged.

## **6.2 MATHEMATICAL MODEL OF PHOTOGRAMMETRIC CONFIGURATION**

Initially, the model chosen to describe the x-ray imaging set-up was the perspective projection using convergent photography with the x-ray source as the focus and the film as the image plane. However, as the project continued, it

became clear that this was not the case. Instead, the three films were exposed at three different exposure stations as if the source was on straight track instead of being rotated through an angle on a gantry (see Figure 6.3). Each image was found to have its perspective centre approximately 12.0 cm apart along the x-axis. Each image also was found to have a different focal length (source to image distance) which reflects the Z-position due to the rotation of the gantry.

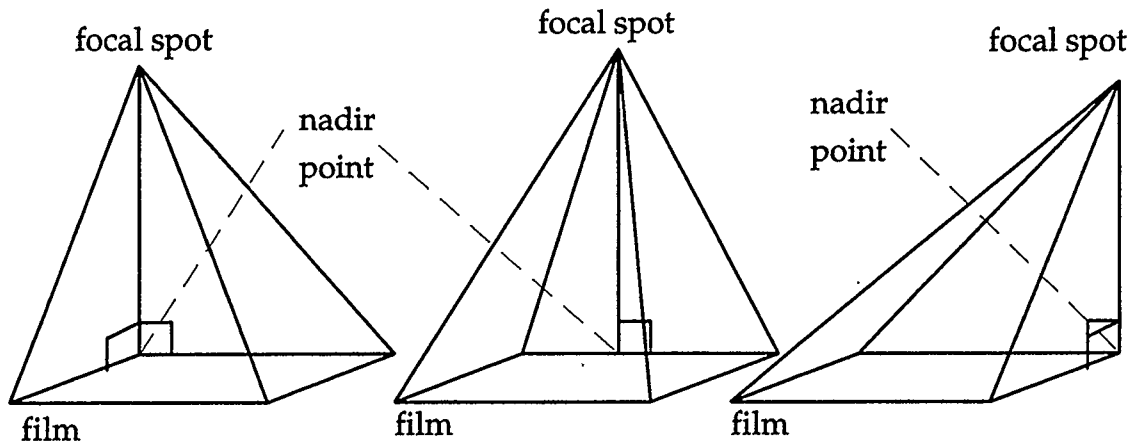


**Figure 6.3**

### **Diagram of Image Acquisition Configuration**

The source for the left image is positioned directly above the film perpendicular to the film plane with the nadir footprint lying on the bottom edge of the film (approximately 10 cm from the centre of the film; see Figure 6.3). The source for the right image was rotated on a gantry through an angle of approximately 15 degrees.

The 15 degree angles used for the image acquisition in this thesis were expected to result in convergent geometry. However, when the principal point was computed, it was found that it coincided with the nadir point (the point in the x-ray film vertically beneath the source/perspective centre). When the image coordinates were adjusted so that the principal point was at the centre of gravity for the image, the model formation and reconstruction process could be completed.

The goal of any stereo imaging process is to see a three-dimensional image either with a mirror stereoscope or as a three-dimensional object rendered on a computer. Convergent photography uses relatively large angles which are very difficult to see stereoscopically. However, texts discussing stereoscopic viewing identify an angle of 16 degrees as the limit of the human eye to focus in three dimensions. Because the angles between any two films is 15 degrees, it may be possible for some people to see the three-dimensional model if the photographs or films are set up with a mirror stereoscope.

The configuration of the imaging system including the specially constructed film table, made the choice of the simplest photogrammetric model possible. This model assumes that one source (left image source) is held stationary and the other source (right image source) is rotated and translated with respect to the left source. The photo coordinates are measured and the object coordinates (object space control = surveyed coordinates on the phantom)

are known. This results in six exterior orientation parameters ( $\omega$ ,  $\phi$ ,  $\kappa$ ,  $X_0$ ,  $Y_0$ ,  $Z_0$ ) which must be resolved to complete the reconstruction process.

The 6 steps needed for the reconstruction of the three-dimensional object are:

1. Calculate the centre of each of the lead pellets which were imaged as circles on the films.
2. Bring all the image coordinates to a common point for each film.
3. Use DLT to bring all images coordinates to principal point of (0,0).
4. Relative orientation using coplanarity condition.
5. Absolute orientation using a 3D similarity transformation.
6. Compare results of DLT and absolute orientation with Bundle adjustment.

### STEP 1

A mathematical model for the calculation of centre coordinates for the imaged spheres was necessary because they could not be accurately determined using only measurements of the centres from the AC1. With the size of the imaged pellets as large circles, 1400 microns in diameter, and the comparatively small target diameter of 40 microns with the Wild AC1, the identification of the centres was subject to error. The distance equation for the radius of a circle was chosen as the mathematical model and the method of least squares was used to determine the best estimate of the centres. The  $x$ ,  $y$  coordinates for four points

around the circumference of each imaged circle were used as the observations for the least squares equations.

The following equation for the radius of a circle was used.

$$radius = \sqrt{(x_i - x_c)^2 + (y_i - y_c)^2} \quad (6.4)$$

Where  $x_i$ ,  $y_i$  are the measured values of the points on the edge of each circle and  $x_c$ ,  $y_c$  are the centre coordinates of the circle.

Figures 6.1 a, b and c show the position of each circle on the films. These figures demonstrate that even when the lead pellets were overlapped on the phantom, the images showed the separation of the pellets. Due to the position of the source, this was even possible for the middle image.

**Table 6.1**  
**Calculated Centre Coordinates and Radii**

Point	Left Film			Middle Film			Right Film		
	X ( $\mu\text{m}$ )	Y ( $\mu\text{m}$ )	R ( $\mu\text{m}$ )	X ( $\mu\text{m}$ )	Y ( $\mu\text{m}$ )	R ( $\mu\text{m}$ )	X ( $\mu\text{m}$ )	Y ( $\mu\text{m}$ )	R ( $\mu\text{m}$ )
1	-28317	-82798	728	-54106	-59000	694	-87878	-70004	688
2	-27804	-23788	750	-51671	-378	701	-82437	-11034	746
3	-26863	37208	738	-52296	60217	722	-83966	50071	767
4	30573	-25256	712	6384	-1957	684	-23947	-13532	688
5	93180	-83625	844	66037	-60161	850	32780	-73049	878
6	89643	-25724	622	65188	-2573	585	35504	-15669	779
7	93432	35616	965	67017	58324	949	36000	46323	958
8	94252	34488	686	68877	57252	603	39016	45148	624
9	93916	-84565	697	67677	-61086	589	35472	-74047	691
10	56464	-92862	696	57298	-69362	669	52507	-82288	613
11	56985	3714	611	58354	27123	566	55442	14249	553
12	88351	-26320	799	64563	-3180	752	35400	-15070	616
13	70668	-35787	733	60198	-12416	727	44592	-25180	696
14	71241	-35391	823	60034	-12064	793	43702	-24773	779
15	-34795	-34132	675	-45637	-10547	650	-62393	-21675	715
16	-41060	-42673	529	-40940	-19022	540	-45953	-30410	579
17	-28012	-24240	808	-51166	-845	744	-81197	-11511	782
18	-35529	-34563	635	-45765	-10971	643	-61802	-22088	617
19	-42277	-43343	622	-41729	-19682	631	-46300	-30999	660
20	-44290	5842	663	-42899	29483	692	-45835	18144	719
21	-29522	36614	662	-54004	59679	635	-84725	49529	744
22	-45048	-91926	626	-44074	-68185	674	-48858	-79522	721
23	6868	-44063	655	7382	-20518	624	2833	-32598	643
	mean	radius	708			688			680
	Standard Deviation		+/-14			+/-9			+/-8



## Step 2

These calculated centre coordinates are used as the two-dimensional positions of the pellet images in the analytical relative orientation procedures for the reconstruction of the model of the phantom. As discussed earlier, the phantom survey resulted in control points on the phantom.

During the measurement of the points with the WILD AC1 Stereo Comparator, the images of the four fiducial marks embedded in the film table were also measured. This provided information for the interior orientation of the system and made the reduction of the images coordinates to the centre of gravity possible.

The average value of the x and y coordinates for the fiducial marks for each separate film were used to bring the points to the film's centre of gravity. The average position of the fiducials are in Table 6.2.

**Table 6.2**  
**Average Values of Fiducials**

Film	X ( $\mu\text{m}$ )	Y ( $\mu\text{m}$ )
Left	3473	-9690
Middle	5561	13883
Right	3032	1806

The film measurements were then reduced to the centre of gravity by subtracting the above values. Normally, the interior orientation parameters (focal length,  $x_p$ ,  $y_p$ ) are determined by using a two-dimensional similarity,

affine or projective transformation. Instead, a DLT was used to recover these parameters. The DLT uses all 23 control points to determine the interior orientation and therefore is highly redundant. If the four fiducials were used, the redundancy would be minimal.

### Step 3

With these adjusted x and y coordinates and the surveyed x, y, z coordinates, a Direct Linear Transformation (DLT) was utilised to adjust the comparator measurements to the principal point.

The first attempt using the DLT resulted in the principal points found in Table 6.3.

**Table 6.3**

**Principal Points Calculated from DLT (first run)**

Film	X <sub>o</sub> (μm)	Y <sub>o</sub> (μm)
Left	-120012	-119115
Middle	2228	-118878
Right	127397	-112787

The image coordinates were reduced by the above values and the DLT was used again to find the new principal point coordinates for each film. The principal points were still not at the centre of the images. The calculated principal points were subtracted from the image coordinates and the DLT was run again until the calculated principal point was close to zero or the centre of

the images. This was performed three times until the desired results were achieved.

The final principal point coordinates to which the comparator data had been adjusted are listed in Table 6.4.

**Table 6.4**

**Principal Points Calculated from DLT (last run)**

FILM	X ( $\mu\text{m}$ )	Y ( $\mu\text{m}$ )
Left	0.0024	-0.0025
Middle	0.0002	0.0003
Right	0.0006	0.0033

The major drawback for the imaging system used for this thesis was the lack of a stereotactic attachment. The specially constructed film table fulfilled its purpose even if it was not as stable as the attachment option specifically designed for the mammography machine would have been. Fiducial marks are utilised in metric cameras to facilitate the interior orientation of the system. The fiducials on the film table were necessary because each new film was placed in the AC1 Stereo Comparator differently causing the measured coordinates to be shifted each time (Figure 6.4). The fiducials on the film table allowed the points on the films to be oriented to a common point. Other methods to avoid this might include a reseau grid or fiducials mounted in the film cassette.

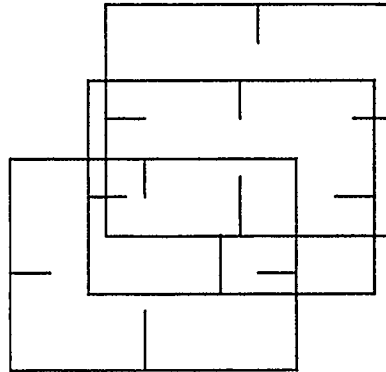


**Figure 6.4**

### **Relative Placement of Films in the Wild AC1 Stereo Comparator**

#### **Step 4**

With the points in a common coordinate system for each film, the next step of the object reconstruction could be approached. This next stage is the relative orientation. It utilises two films at a time for the mathematical construction of a stereo model. Three models are possible from the configuration of the image acquisition.

The coplanarity condition equation was chosen as the mathematical model for relative orientation. In using the coplanarity equation, the points which are common to both films, the x-ray sources or foci and the model point, must all lie in the same plane. The coplanarity condition equation is defined as follows:

$$(A \times B) \cdot C = 0 \quad \text{Where } A, B \text{ and } C \text{ are vectors.} \quad (6.5)$$

$A \times B$  results in a vector that is perpendicular to both vectors  $A$  and  $B$ .

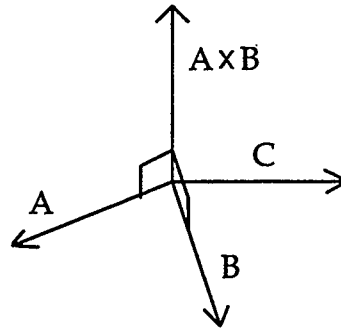


Figure 6.5

Vector of  $A \times B$

$(A \times B) \cdot C = 0$  only if  $A \times B$  is orthogonal to  $C$ . The dot product of two vectors is a scalar in the form of equation 6.6.

$$A \times B \cdot C = \|A \times B\| \cdot \|C\| \cos \theta = 0 \quad (6.6)$$

where  $\theta$  is the angle between the two vectors  $A \times B$  and  $C$

If  $\theta$  is  $90^\circ$  (i.e.,  $C$  is perpendicular to  $A \times B$ ),  $\cos \theta = \cos 90^\circ = 0$  and vector  $C$  is in the same plane as vectors  $A$  and  $B$  (see Figure 6.6).

Therefore, this equation may be used as a constraint to force vector  $C$  to lie in the same plane as vectors  $A$  and  $B$ .

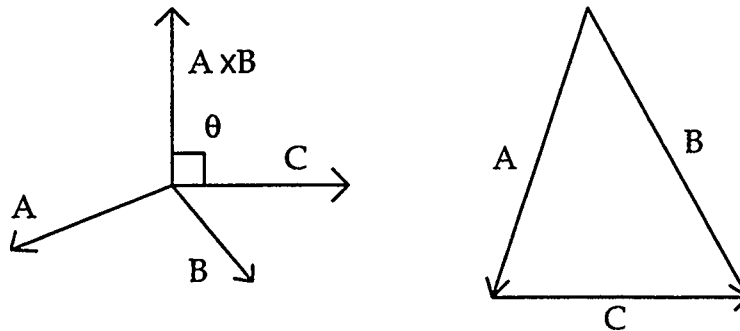


Figure 6.6  
Diagram of Geometry of  $A \times B \cdot C$

The relative orientation procedure, using the coplanarity equations, results in the reconstruction of a three-dimensional model. The scale of the model still needs to be determined. If the actual photobase is used, the model will be very close to the actual object size and the scale will be close to unity.

The Equation 6.6 for coplanarity can be expressed as a determinant (i.e., Equation. 6.7). The first line of the determinant is equivalent to the vector between the two x-ray sources. The second line of the determinant represents the vector of the left-hand image x and y coordinates and the focal length is the z component. The last line of the determinant represents the vector from the right-hand source to the model point (i.e., vector B in Figure 6.6). This vector is composed of the rotated values of the right-hand image x and y coordinates and z value (e.g., the focal length). The order of rotation used for this thesis is  $\kappa, \phi, \omega$ . The standard order of rotation is  $\omega, \phi, \kappa$  [Cosandier, 1992].

If all three vectors lie in the same plane, the determinant will be zero. This constraint is necessary for a unique solution of the model points.

$$\begin{vmatrix} bx & by & bz \\ x_1 & y_1 & f_1 \\ \bar{x} & \bar{y} & \bar{z} \end{vmatrix} = 0 \quad (6.7)$$

Where  $\bar{x}, \bar{y}$  and  $\bar{z}$  are the transformed coordinates for the right image's perspective centre. The source to image distance for the right image is  $f_r$ .

$$\bar{x} = m_{11}x_r + m_{12}y_r - m_{13}f_r \quad (6.8a)$$

$$\bar{y} = m_{21}x_r + m_{22}y_r - m_{23}f_r \quad (6.8b)$$

$$\bar{z} = m_{31}x_r + m_{32}y_r - m_{33}f_r \quad (6.8c)$$

The rotation matrix elements are:

$$m_{11} = \cos \phi * \cos \kappa$$

$$m_{12} = \cos \omega * \sin \kappa + \sin \omega * \sin \phi * \cos \kappa$$

$$m_{13} = \sin \omega * \sin \kappa - \cos \omega * \sin \phi * \cos \kappa$$

$$m_{21} = -\cos \phi * \sin \kappa$$

$$m_{22} = \cos \omega * \cos \kappa - \sin \omega * \sin \phi * \sin \kappa$$

$$m_{23} = \sin \omega * \cos \kappa + \cos \omega * \sin \phi * \sin \kappa$$

$$m_{31} = \sin \phi$$

$$m_{32} = -\sin \omega * \cos \phi$$

$$m_{33} = \cos \omega * \cos \phi$$

Separate source to image distances were used for each image (i.e.,  $f_{left}$ ,  $f_{middle}$  and  $f_{right}$ ).

The determinant (Equation 6.7) must be linearised and this is accomplished by differentiation. Because of the linearisation of the determinant, the solutions must be iterated until the change in the unknowns goes to zero.

The unknowns for relative orientation, if the left source is held stationary and the x component of the photobase is used as  $b_x$ , are:  $b_y$ ,  $b_z$ ,  $\omega$ ,  $\phi$ , and  $\kappa$ . They can be solved by summing the changes in the unknowns at each iteration until convergence is achieved. The unknowns were solved by applying the method of least squares.

The A and B vectors must be scaled to form the model coordinates. These scale factors were determined with Equations 6.9 and 6.10.

$$\lambda = \frac{bx \cdot \bar{z} - bz \cdot \bar{x}}{x_1 \cdot \bar{z} - f_1 \cdot \bar{x}} \quad (6.9)$$

$$\mu = \frac{bx \cdot z_1 - bz \cdot x_1}{x_1 \cdot \bar{z} - f_1 \cdot \bar{x}} \quad (6.10)$$

The scale factors  $\lambda$  and  $\mu$  are then applied to the model coordinates.

### Step 5

The final step of the object reconstruction is the absolute orientation to bring the three-dimensional model coordinates into the ground coordinate system. To do this, the survey coordinates, obtained from the microsurvey, are used as control points and the model coordinates are scaled, rotated and translated to fit that system.

The mathematical model for absolute orientation consists of the collinearity equations. They are used to determine the final scaled object coordinates as follows:

$$X_g = \lambda M X_m + \Delta X_g \quad (6.11)$$

where:

- $X_g$  is the vector of control point values
- $\lambda$  is the scale factor
- $M$  is the rotation matrix combining the  $\omega$   $\pi$   $\kappa$  rotations
- $X_m$  is the vector of model coordinates as determined from the relative orientation process
- $\Delta X_g$  is the vector of translations from model space to control space.



The primary reason that the three steps of interior, relative and absolute orientation were chosen versus the self-calibrating Bundle Adjustment or the interior and exterior orientation using the collinearity equations, was for the added robustness of the process. This robustness is directly related to the opportunity to check the results at each step of the reconstruction process thus allowing any blunders to be corrected before continuing to the next step.

### **Step 6**

Finally, a self calibrating Bundle Adjustment supplied by Hamid Ebadi of the Geomatics Engineering Department at the University of Calgary, was used to confirm the results obtained and the assumptions made for this research. These included the focal lengths, the principal points of each image, the perspective centres, and the rotation angles. The results of the Bundle Adjustment are found in Section 6.3.

## **6.3 MATHEMATICAL RECONSTRUCTION OF THE MODEL**

The mathematical reconstruction of the model is based on the three-dimensional coordinates resulting from the measured two-dimensional image coordinates and the geometry of the imaging system. In this section, the analytically determined coordinates of the phantom and the microsurvey phantom coordinates are compared. The deviation of the calculated from the

surveyed coordinates gives the measure of accuracy and precision of the procedure.

Below are the results of the analytical photogrammetric techniques and the comparison to the surveyed values of the phantom coordinates. The three-dimensional coordinates were calculated using the three different methods of DLT, 3-D Similarity transformation and Bundle Adjustment. A comparison of the results shows that all three methods are within the 0.6 mm.

The DLT results, which confirmed that analytical photogrammetry could be used directly for x-ray images, are listed in Table 6.5. These values were adjusted for the centre of gravity before being introduced into the DLT program.

The results of the analytical relative orientation are given in Tables 6.7, 6.8 and 6.9. The parallax values ( $P_y$ ) indicate that the choice of mathematical model was appropriate (i.e., a good fit).

Table 6.10 shows the results of the absolute orientation with the associated rms values.

Table 6.5

## Image Coordinates Corrected for Centre of Gravity and Principal Point Shift

Point	Left Film		Middle Film		Right Film	
	X ( $\mu\text{m}$ )	Y ( $\mu\text{m}$ )	X ( $\mu\text{m}$ )	Y ( $\mu\text{m}$ )	X ( $\mu\text{m}$ )	Y ( $\mu\text{m}$ )
1	88228	46007	-61892	45985	-218302	40979
2	88741	105018	-59456	104607	-212861	99949
3	89682	166014	-60081	165202	-214390	161054
4	147118	103550	-1401	103027	-154372	97451
5	209725	45181	58252	44824	-97644	37934
6	206188	103082	57403	102411	-95024	95913
7	209977	164421	59231	163309	-94424	157306
8	210797	163294	61091	162237	-91408	156131
9	210461	44241	59891	43899	-94952	36936
10	173009	35944	49513	35623	-77917	28695
11	173530	132520	50569	132108	-74982	125231
12	204896	102485	56778	101805	-94920	95314
13	187213	93019	52413	92569	-85832	85803
14	187786	93414	52249	92921	-86722	86210
15	81750	94674	-53423	94438	-192817	89308
16	75485	86133	-48725	85963	-176377	80573
17	88533	104566	-58951	104140	-211621	99472
18	81016	94243	-53551	94014	-192227	88895
19	74268	85463	-49514	85303	-176725	79984
20	72255	134647	-50684	134467	-176259	129127
21	87023	165419	-61789	164664	-215150	160512
22	71497	36880	-51859	36799	-179282	31461
23	123413	84743	-403	84467	-127591	78385

The reconstructed object coordinates as derived from the DLT are listed in Table 6.6. As can be seen from the last four columns in Table 6.6, the mathematical model fits the data very well.

Table 6.6

## DLT Results Using All Three films

Point	X(mm)	Y(mm)	Z(mm)	rms x	rms y	rms z	rms vector
1	-0.217	0.097	0.092	0.036	0.032	0.133	0.141
2	0.639	48.431	-4.229	0.009	0.012	0.043	0.045
3	0.303	96.157	1.944	0.003	0.007	0.017	0.019
4	48.155	47.662	-5.054	0.005	0.008	0.024	0.025
5	96.897	0.071	0.165	0.009	0.009	0.042	0.044
6	96.330	47.762	-6.203	0.007	0.012	0.034	0.037
7	96.722	95.564	0.799	0.009	0.025	0.045	0.052
8	98.531	95.666	-2.333	0.006	0.015	0.028	0.033
9	98.499	-0.414	-2.608	0.014	0.014	0.067	0.070
10	97.160	0.240	-97.137	0.017	0.015	0.085	0.088
11	97.268	95.199	-96.589	0.015	0.034	0.077	0.086
12	96.005	47.675	-8.218	0.007	0.012	0.033	0.036
13	95.890	47.939	-51.467	0.009	0.015	0.046	0.049
14	95.539	47.800	-48.87	0.004	0.007	0.022	0.024
15	0.710	48.077	-47.188	0.017	0.024	0.096	0.101
16	0.401	47.866	-90.476	0.014	0.021	0.089	0.092
17	0.781	48.491	-6.341	0.010	0.014	0.048	0.051
18	0.354	48.124	-49.471	0.012	0.018	0.073	0.076
19	-0.564	47.544	-92.300	0.006	0.010	0.041	0.043
20	-2.500	96.264	-94.355	0.007	0.016	0.047	0.050
21	-1.443	96.550	-0.734	0.006	0.013	0.031	0.035
22	-2.679	0.338	-95.717	0.026	0.024	0.169	0.173
23	47.554	47.263	-93.163	0.006	0.008	0.029	0.031
			rms	0.250	0.176	0.276	0.412

The results of the analytical relative orientation are given in Tables 6.7, 6.8 and 6.9.

**Table 6.7**

**Model Coordinates Using Left and Right Film**

Point	X (mm)	Y (mm)	Z (mm)	py (mm)
1	6.953	3.629	-42.426	-0.008
2	7.075	8.371	-42.922	0.003
3	7.061	13.072	-42.388	-0.003
4	11.726	8.252	-42.912	0.002
5	16.450	3.545	-42.228	-0.000
6	16.438	8.217	-42.922	0.003
7	16.501	12.921	-42.307	-0.002
8	16.685	12.926	-42.613	-0.002
9	16.613	3.493	-42.498	-0.001
10	16.614	3.453	-51.702	-0.003
11	16.700	12.756	-51.811	-0.005
12	16.411	8.207	-43.122	0.004
13	16.462	8.178	-47.340	0.002
14	16.425	8.169	-47.089	0.002
15	7.155	8.283	-47.121	0.007
16	7.199	8.211	-51.346	0.007
17	7.092	8.374	-43.127	0.004
18	7.125	8.286	-47.348	0.005
19	7.108	8.179	-51.524	0.000
20	6.953	12.958	-51.811	-0.002
21	6.894	13.108	-42.652	-0.006
22	6.877	3.550	-51.785	-0.006
23	11.807	8.107	-51.508	0.001

Table 6.8

## Model Coordinates Using Left and Middle Film

Point	X (mm)	Y (mm)	Z (mm)	py (mm)
1	6.910	3.605	-42.168	-0.003
2	7.034	8.324	-42.677	0.001
3	7.026	13.007	-42.179	-0.000
4	11.662	8.209	-42.677	-0.000
5	16.353	3.522	-41.979	0.001
6	16.351	8.174	-42.693	0.000
7	16.424	12.860	-42.111	0.000
8	16.603	12.862	-42.404	-0.001
9	16.509	3.470	-42.231	0.000
10	16.509	3.431	-51.373	-0.003
11	16.602	12.678	-51.507	-0.000
12	16.320	8.162	-42.883	0.002
13	16.367	8.134	-47.069	-0.003
14	16.329	8.123	-46.816	0.000
15	7.112	8.237	-46.839	0.000
16	7.153	8.161	-51.018	0.003
17	7.052	8.328	-42.886	0.003
18	7.081	8.237	-47.052	0.000
19	7.062	8.126	-51.196	0.002
20	6.911	12.878	-51.494	0.000
21	6.861	13.044	-42.448	-0.003
22	6.830	3.524	-51.429	-0.002
23	11.735	8.057	-51.191	0.002

Table 6.9

## Model Coordinates Using Middle and Right Film

Point	X (mm)	Y (mm)	Z (mm)	py (mm)
1	-4.928	3.664	-43.970	-0.005
2	-4.787	8.422	-44.465	0.002
3	-4.777	13.137	-43.910	-0.002
4	-0.113	8.291	-44.446	0.003
5	4.617	3.554	-43.765	-0.004
6	4.621	8.242	-44.451	0.003
7	4.700	12.959	-43.818	-0.002
8	4.883	12.966	-44.136	-0.000
9	4.778	3.503	-44.052	-0.001
10	4.779	3.438	-53.299	-0.000
11	4.890	12.778	-53.406	-0.005
12	4.592	8.232	-44.661	0.002
13	4.641	8.195	-48.902	0.005
14	4.603	8.186	-48.653	0.002
15	-4.710	8.323	-48.691	0.007
16	-4.672	8.240	-52.950	0.004
17	-4.768	8.423	-44.666	0.000
18	-4.745	8.328	-48.931	0.005
19	-4.764	8.208	-53.128	-0.002
20	-4.903	13.008	-53.417	-0.003
21	-4.942	13.172	-44.169	-0.003
22	-5.015	3.560	-53.403	-0.003
23	-0.039	8.123	-53.104	-0.002

The combined results from the analytical photogrammetry techniques of Relative and Absolute Orientation are found in Table 6.10.

**Table 6.10**

**Final Results of Absolute Orientation**

Pt.	Left and Right			Left and Middle			Middle and Right		
	X(mm)	Y(mm)	Z(mm)	X(mm)	Y(mm)	Z(mm)	X(mm)	Y(mm)	Z(mm)
1	-0.023	-0.144	0.061	-0.130	-0.388	0.019	-0.007	0.025	0.009
2	0.714	48.392	-4.359	0.615	48.278	-4.433	0.779	48.464	-4.360
3	0.263	96.361	1.764	0.183	96.378	1.492	0.446	96.304	1.953
4	48.256	47.598	-5.170	48.246	47.533	-5.290	48.298	47.680	-5.090
5	97.072	-0.179	0.243	97.083	-0.362	0.240	97.034	0.007	0.233
6	96.411	47.659	-6.191	96.495	47.632	-6.309	96.402	47.742	-6.062
7	96.755	95.662	0.741	96.920	95.763	0.471	96.787	95.600	1.037
8	98.578	95.765	-2.419	98.705	95.847	-2.573	98.582	95.743	-2.233
9	98.693	-0.661	-2.554	98.647	-0.840	-2.390	98.621	-0.460	-2.724
10	96.924	0.218	-96.614	96.983	0.308	-96.462	96.841	0.196	-96.689
11	96.958	95.307	-96.433	97.054	95.501	-96.279	96.880	95.145	-96.461
12	96.097	47.584	-8.229	96.148	47.535	-8.255	96.069	47.673	-8.189
13	95.797	47.883	-51.347	95.875	47.957	-51.342	95.753	47.896	-51.301
14	95.466	47.755	-48.774	95.528	47.798	-48.733	95.415	47.765	-48.767
15	0.726	48.085	-47.296	0.666	48.090	-47.291	0.749	48.072	-47.332
16	0.361	47.944	-90.482	0.331	48.019	-90.307	0.320	47.836	-90.634
17	0.848	48.457	-6.459	0.760	48.354	-6.588	0.935	48.504	-6.409
18	0.375	48.146	-49.608	0.300	48.121	-49.477	0.352	48.148	-49.762
19	-0.606	47.631	-92.294	-0.633	47.682	-92.133	-0.641	47.519	-92.432
20	-2.655	96.504	-94.520	-2.687	96.624	-94.356	-2.663	96.328	-94.643
21	-1.495	96.748	-0.894	-1.565	96.789	-1.236	-1.283	96.675	-0.641
22	-2.607	0.342	-95.562	-2.639	0.343	-95.273	-2.715	0.297	-95.839
23	47.429	47.320	-93.047	47.455	47.417	-92.935	47.386	47.214	-93.107

The Bundle Adjustment was used to recover the interior and exterior orientation parameters. This is desirable because the physical measurement of a focal length, or in this case, the source to image distance, is very difficult to



determine due to the housing around the x-ray source. The exterior and interior orientation parameters are shown in Tables 6.11 and 6.12.

**Table 6.11**

**Exterior Orientation Parameters from Bundle Adjustment**

Photo	Xo (m)	Yo (m)	Zo (m)	Kappa (radians)	Phi (radians)	Omega (radians)
Left	-0.061	-0.044	0.431	0.009	0.014	0.018
Middle	0.059	-0.044	0.444	0.011	0.013	0.015
Right	0.184	-0.040	0.424	0.027	0.014	0.017

**Table 6.12**

**Interior Orientation Parameters**

Film	Focal (mm)	xo (mm)	yo (mm)
Left	536.863	3.984	1.972
Middle	550.795	3.085	-1.130
Right	532.342	1.925	-5.255

The physical measurement for the source to image distance, utilising a cloth tape, was 60 cm. The location of the x-ray source was not clearly determined. The focal lengths in Table 6.12 correspond to the source to image distances for the three films as computed by the Bundle Adjustment [Ebadi, 1995]. Therefore, the values recovered using the Bundle Adjustment are deemed to be more reliable than the physical measurements.

Table 6.13 provides a comparison of the three reconstruction methods employed in this thesis for the mathematical model fit. Table 6.14 shows the expected accuracy of the different models.

**Table 6.13**  
**Mathematical Model Fit**

<b>Model</b>	<b># Control Points</b>	<b>Xrms (mm)</b>	<b>Yrms (mm)</b>	<b>Zrms (mm)</b>	<b>RMS Vector</b>
<b>DLT (3 films)</b>	23	0.250	0.176	0.276	0.412
<b>Absolute Orientation (avg of 3 films)</b>	23	0.289	0.234	0.323	0.494
	18	0.286	0.258	0.347	0.521
	5	0.290	0.303	0.314	0.530
<b>Bundle Adjustment (3 films)</b>	23	0.243	0.199	0.191	0.368
	18	0.224	0.193	0.210	0.363
	5	0.126	0.110	0.126	0.209

**Table 6.14**  
**Accuracy of the Models**

<b>MODEL</b>	<b># Tie Points</b>	<b>Xrms (mm)</b>	<b>Yrms (mm)</b>	<b>Zrms (mm)</b>	<b>RMS Vector</b>
<b>DLT (3 films)</b>	N/A	N/A	N/A	N/A	N/A
<b>Absolute Orientation (avg of 3 films)</b>	0	N/A	N/A	N/A	N/A
	5	0.343	0.158	0.157	0.412
	18	0.380	0.334	0.334	0.607
<b>Bundle Adjustment (3 films)</b>	0	N/A	N/A	N/A	N/A
	5	0.329	0.165	0.104	0.382
	18	0.329	0.316	0.380	0.594

Table 6.14 compares the Bundle Adjustment results with the Absolute Orientation results. As indicated in the table, the Absolute Orientation uses the average value obtained during Relative Orientation. The Relative Orientation procedure utilises only two images to form each of the three-dimensional models. Therefore, three different models are constructed. The Bundle Adjustment, however, uses all three images simultaneously and, thus, has a stronger geometry with which to compute the check points.

## CHAPTER SEVEN

### CONCLUSIONS AND RECOMMENDATIONS

#### 7.1 CONCLUSIONS

The application of photogrammetry to stereo mammographic images was successful. The ability to reconstruct the phantom within 0.5 mm is far better than that of the few centimetres accuracy possible with the current methods of mammography. These methods should be applicable to the problem of calcification classification that is being addressed by Liang Shen in the Electrical Engineering Department at the University of Calgary.

Different magnifications or scales were expected in the x and y directions due to the heel effect during the production of the x-rays. However, this was only noticed in the higher y rms values from the Bundle Adjustment.

X-ray images are created by the higher density object leaving a shadow on the film. The edges of the shadows are fuzzy making the manual measurement unreliable. For this thesis, the measurement of the four quadrants of the imaged circles was sufficient to locate the circle centres to be used in the subsequent calculations.

A phantom in the shape of a cube constructed of Plexiglas and lead pellets was sufficient for determining the advantages of photogrammetry in mammography. It has been shown that photogrammetry is capable of resolving ambiguities in overlapping features.

The phantom pellets were not labelled in the x-ray images and experience in dealing with photographs and points sources proved essential in identifying the shadows on the films correctly. Labelling is a major cause of blunders. The DLT was useful in detecting this type of blunder. Large rms values indicated potential blunders. Only two points had large rms values and it was found that they had been misidentified. A better method of labelling the features is required.

This method of stereomammography is most appropriate for use in the diagnosis of a suspected malignancy or in the treatment planning for a known cancerous tumour or cluster of calcifications. Photogrammetry was successfully applied to stereomammography to give a depth map of a phantom representing the female breast. The precision is higher than what is possible with the current techniques but without a reference system, the accuracy is still questionable.

There were a few unexpected results from this research. The perspective centre was not directly above the centre of the image but was off the edge in the negative y direction indicating that the focal spot was not situated directly over the film as was assumed. Once this was recognised and the images corrected for the principal point shift, the rest of the computations were facilitated.

The heel effect, which is a result of a drop off of x-ray intensity away from the anode direction, was not as noticeable as was expected.

A convergent photographic configuration was expected. This proved to be an incorrect assumption. Instead, the images were created as if the x-ray source was on a track instead of a rotating gantry. This helped in the final determination of the object reconstruction parameters.

No grid was used for this thesis work. Scattering of x-rays is greater without a grid but the radiation dose can be decreased for the same image quality.

Image quality is affected by patient movement and compression, x-ray scatter (noise), film unflatness (minimal) and radiation dosage which is related to the attenuation coefficients of the objects of interest. For the constructed phantom, patient movement and compression were not factors. The film unflatness and the radiation dosage is the same as it would be for clinical mammograms. Therefore, the image quality could only be degraded by scatter due to the absence of a grid.

## **7.2 RECOMMENDATIONS**

Suggested changes to machinery and protocol include a standard stereotactic attachment. With this attachment, the radiation source appears to move laterally to the image plane even when it is rotated around the object (i.e., parallel to the object/film plane) making the use of photogrammetry viable.

To improve the object reconstruction process, an extra film can be used giving the system more redundancy and therefore better accuracy. However, a

lower radiation dose is required for this option which might affect the image quality.

Digital images are necessary if automatic recognition techniques are to be employed. Photogrammetric software that uses digital images has already been developed. The biggest concern is to achieve high resolution without requiring large image files so that a personal computer can be used. This is more economical than using a SUN workstation or UNIX based machine. However, if the computer is used only for diagnosis and treatment of one patient at a time and is dedicated to that use, larger image files could be used. The stereotactic machine in Edmonton uses digital images but the resolution of these images is poorer than the resolution for conventional mammographic films due to the method of viewing the mammograms on a CRT screen. This method is affected by distortions in the display of the images.

A fiducial system is needed to enhance the accuracy of the reconstruction unless a self-calibrating program is used to determine the interior orientation of the system. To remove or reduce human error, automation of image matching and object identification are needed. Labelling or clear identification of the points is necessary to minimise blunders.

Finally, a reference system is needed to improve the accuracy of the determination of any points on a mammogram. As a start, fiducials in the film cassette would be beneficial. Another possibility is a reference frame that is

fixed on the patient. The deformability of the breast presents a challenge for the design of a reference system. This was beyond the scope of this thesis but is considered to be the most important hurdle to overcome.

Future work that would enhance the precision of measurements made on mammographic films includes the determination of distortions present due to the imaging process. The correction for these error sources along with a reference system could greatly improve the precision and accuracy of feature identification and location. This would facilitate treatment planning and diagnosis.



## REFERENCES

- American Society for Photogrammetry and Remote Sensing, [1979], "*Chapter 12, X-Ray Photogrammetry Systems and Applications*", Non-Topographic Photogrammetry, Second Edition, Falls Church.
- ASP, (American Society for Photogrammetry and Remote Sensing), [1980], "*Manual of Photogrammetry*", Fourth Edition, 105 N. Virginia Ave., Falls Church, Va. 22046, Chapter 6.
- Barnes Gary T.; Frey, G. Donald, [1991] "*Screen Film Mammography, Imaging Considerations and Medical Physics Responsibilities*", Proceedings of SEAAPM Spring Symposium in Columbia, South Carolina, pp. 1-142.
- Bassett, Lawrence W., [1992], "*Mammographic Analysis of Calcifications*", Radiologic Clinics of North America, Volume 30, Number 1 pp. 93-105.
- Bryant, Heather E.; Brasher, Penny M.A., [1994, January], "*Risks and Probabilities of Breast Cancer: Short-Term versus Lifetime Probabilities*", Canadian Medical Association Journal, Volume 150, Number 2, pp. 211-216.
- Chelberg, David M.; Hsu, Jean; Babbs, Charles F.; Pizlo, Zygmunt; Delp, Edward J., [1994], "*Digital Stereomammography*", Elsevier Science B. V., pp. 181-190.
- Christenson, Edward E.; Curry, Thomas S.; Dowdey, James E., [1978], "*An Introduction to the Physics of Diagnostic Radiology*", Lea & Febiger, Philadelphia, USA.

- Ciatto, Stefano; Cataliotti, Luigi; Distante, Vito, [1987], "*Nonpalpable Lesions Detected with Mammography: Review of 512 Consecutive Cases*", *Radiology*, 165, pp. 99-102.
- Cosandier, D., [1992], "*Analytical Relative Orientation*", Seminar for ENGO 541, Department of Geomatics Engineering, The University of Calgary, Calgary, Alberta, Canada, T2N 1N4.
- Ebadi, Hamid, [1995], Bundle Adjustment - Optimisation Computer Program, Department of Geomatics Engineering, The University of Calgary, Calgary, Alberta, Canada, T2N 1N4.
- Eisberg, Robert Martin, [1961] "*Fundamentals of Modern Physics*", John Wiley and Sons, USA.
- Fletcher, Suzanne W.; Black, William; Harris, Russel; Rimer, Barbara K.; Shapiro, Sam, [1993, October 20], "*Special Article Report on the International Workshop on Screening for Breast Cancer*", *Journal of the National Cancer Institute*, Volume 85, Number 20, pp. 1644-1656.
- Franceschi, Dido et al, [1990], "*Biopsy of the Breast for Mammographically Detected Lesions*", *Surgery Gynecology and Obstetrics*, Volume 171, Number 6, December, pp. 449-455.
- Ghosh, Sanjib K., [1979], "*Analytical Photogrammetry*", Second Edition, Pergamon Press Inc., USA., pp. 181-186.

- Hallert, Bertil, [1970], *"X-Ray Photogrammetry"*, Elsevier Publishing Company, Amsterdam.
- Hendrick, R. Edward; Parker, Steve H., *"Stereotaxic Imaging"*, University of Colorado Health Sciences Centre, Denver and Diagnostic Imaging Associates, Englewood, Colorado.
- Karellas, Andrew; Liu, Hong; Harris, Lisa J.; D'Orsi, Carl J.; [1994], *"Digital Mammo Delivers Quick, Reliable Images"*, Breast Imaging, Miller Freeman Inc.
- Kratky, V., [1975], *"Analytical X-Ray Photogrammetry in Scoliosis"*, Photogrammetria, Volume 31, pp 195-210.
- Krupinski, E.A.; Roehrig, H., [1994], *"Comparison of Digital X-Ray Cameras for Stereotactic Breast Needle Biopsy: An Observer Performance Study"*, Elsevier Science B. V, pp. 191-197.
- de Lafontan, Brigitte; et al, [1994], *"Isolated Clustered Microcalcifications: Diagnostic Value of Mammography--Series of 400 Cases with Surgical Verification"*, Radiology, 190: 479-483.
- Long, Shirley M., [1990], *"Handbook of Mammography"*, Mammographic Consulting Services/ Convention Graphics, Edmonton, Alberta, Canada.
- LORAD Medical Systems, [1992]. *"M-III Operators Manual"*, Eagle Road, Commerce Park, Danbury, CT, USA 06810 pp. 1-18.

- McNeil, Gomer T., [1966], "*X-Ray Stereo Photogrammetry*", Photogrammetric Engineering, Volume 32, pp. 993-1004.
- Physical Science Study Committee, [1965], "*Physics*", D.C. Heath and Company under arrangement with Education Development Center, United States of America.
- Renner, W.D., [1977], "*A Photogrammetric Technique for use in Radiation Therapy*", Photogrammetric Engineering and remote Sensing, Volume 43, Number 5, pp. 581-591.
- Shen, Liang, [1992], "*Shape Analysis of Mammographic Calcifications*", Master's Thesis, Department of Electrical Engineering, The University of Calgary, Calgary, Alberta, Canada, T2N 1N4.
- Shen, Liang; Rangayyan, Rangaraj M.; Desautels, J.E. Leo, [1993], "*Detection and Classification of Mammographic Calcifications*", International Journal of Pattern Recognition and Artificial Intelligence, Volume 7, Number 6, pp. 1403-1410.
- Sickles, E.A., [1986], "*Breast Calcifications: Mammographic Evaluation*", Radiology, 160: 289-293.
- Sivaramakrishna, R.; Gordon R., [1995], "*At what size should tumors be detected? A quantitative analysis*", submitted.
- Sprawls, Perry Jr., [1977], "*The Physical Principles of Diagnostic Radiology*", University Park Press, Baltimore, Maryland, USA.

Tipler, Paul A., [1969], *"Foundations of Modern Physics"*, Worth Publishers Inc.

Veress, S.A.; Lippert, F.G.; Takamoto, Takenori, [1977], *"An Analytical Approach to X-Ray Photogrammetry"*, *Photogrammetric Engineering and Remote Sensing*, Volume 43, Number 12, pp. 1503-1510.

Wehr, M. Russel; Richards, James A., [1967], *"Physics of the Atom"*, Addison-Wesley Publishing Company, Inc . USA.

Zhou, Xiaohua; Gordon, Richard, [1989], *"Detection of Early Breast Cancer: An Overview and Future Prospects"*, *Critical Reviews in Biomedical Engineering*, Volume 17, Issue 3, pp. 203-255.